

Condensin dysfunction is a reproductive isolating barrier in mice

<https://doi.org/10.1038/s41586-023-06700-6>

Warif El Yakoubi¹ & Takashi Akera¹✉

Received: 3 November 2022

Accepted: 2 October 2023

Published online: 1 November 2023

 Check for updates

Reproductive isolation occurs when the genomes of two populations accumulate genetic incompatibilities that prevent interbreeding^{1,2}. Understanding of hybrid incompatibility at the cell biology level is limited, particularly in the case of hybrid female sterility³. Here we find that species divergence in condensin regulation and centromere organization between two mouse species, *Mus musculus domesticus* and *Mus spretus*, drives chromosome decondensation and mis-segregation in their F₁ hybrid oocytes, reducing female fertility. The decondensation in hybrid oocytes was especially prominent at pericentromeric major satellites, which are highly abundant at *M. m. domesticus* centromeres^{4–6}, leading to species-specific chromosome mis-segregation and egg aneuploidy. Consistent with the condensation defects, a chromosome structure protein complex, condensin II^{7,8}, was reduced on hybrid oocyte chromosomes. We find that the condensin II subunit NCAPG2 was specifically reduced in the nucleus in prophase and that overexpressing NCAPG2 rescued both the decondensation and egg aneuploidy phenotypes. In addition to the overall reduction in condensin II on chromosomes, major satellites further reduced condensin II levels locally, explaining why this region is particularly prone to decondensation. Together, this study provides cell biological insights into hybrid incompatibility in female meiosis and demonstrates that condensin misregulation and pericentromeric satellite expansion can establish a reproductive isolating barrier in mammals.

Hybrid incompatibility is the genetic cause of postzygotic reproductive isolation, contributing to the speciation process¹. Such incompatibilities arise when the genomes of two closely related species or strains take distinct evolutionary trajectories, resulting in incompatible genomic interactions in F₁ hybrids that are lethal or lead to sterility². Several hybrid incompatibility genes have been identified to explain hybrid lethality and hybrid male sterility^{3,9–11}. Although hybrid female mice and *Drosophila* exhibit fertility issues, facilitating reproductive isolation^{12,13}, the molecular mechanisms underlying hybrid female sterility are unclear.

Female meiosis I division is a highly error-prone process in many mammalian species, affecting fertility^{14–21}. This error-prone nature implies that even the slightest form of hybrid incompatibility in this cell division can have a profound impact on reproduction. Female hybrid mice between *M. m. domesticus* (hereafter, *domesticus*) and *M. spretus* (hereafter *spretus*) are subfertile due to chromosome segregation errors in meiosis I, creating aneuploid eggs^{18,22} (Fig. 1a; see the ‘Mouse strains’ section of the Methods). Such meiotic failures would substantially contribute to maintaining reproductive isolation between these species. However, the molecular basis underlying hybrid incompatibility in the chromosome segregation process remained unclear.

Centromere stretching in hybrid oocytes

To understand the cell biological mechanism underlying reduced fertility in the *domesticus* × *spretus* hybrid female mice, we imaged

chromosome dynamics live in their oocytes. We found that chromosomes lagged in anaphase I more frequently in hybrid oocytes compared with in pure *domesticus* and *spretus* oocytes, consistent with the higher aneuploid egg rate observed in this hybrid^{18,22} (Fig. 1b (top right) and Extended Data Fig. 1a). As centromere evolution can impact the chromosome segregation fidelity and centromere DNA has substantially diverged between *domesticus* and *spretus*, we examined whether chromosomes from one parent could be more prone to segregation errors in this hybrid. Taking advantage of *spretus* centromeres, which have substantially more centromeric minor satellites and fewer pericentromeric major satellites compared with *domesticus* centromeres^{5,6} (Fig. 1a), we can distinguish between *domesticus* and *spretus* centromeres using specific transcription activator-like effector (TALE) constructs^{4,23}. Differential labelling of parental chromosomes revealed that it was predominantly *domesticus* chromosomes that were lagging in hybrid oocytes (Fig. 1b (bottom right)). To understand the mechanisms behind this species-specific chromosome mis-segregation, we analysed their chromosome morphology in prometaphase I and metaphase I (Fig. 1c and Extended Data Fig. 1b–d). In *domesticus* oocytes, sister chromatids were individualizing in prometaphase I with some centromeres still partially decondensed and stretched (Fig. 1c (*domesticus*, white arrowhead)). Chromosomes progressively condensed over time, and most centromeres were properly condensed by metaphase I in *domesticus* oocytes. By contrast, hybrid oocytes showed significant chromosome decondensation manifested by their shorter and wider chromosomes and less individualization of the chromosomes

¹Cell and Developmental Biology Center, National Heart, Lung, and Blood Institute, National Institutes of Health, Bethesda, MD, USA. ✉e-mail: takashi.akera@nih.gov

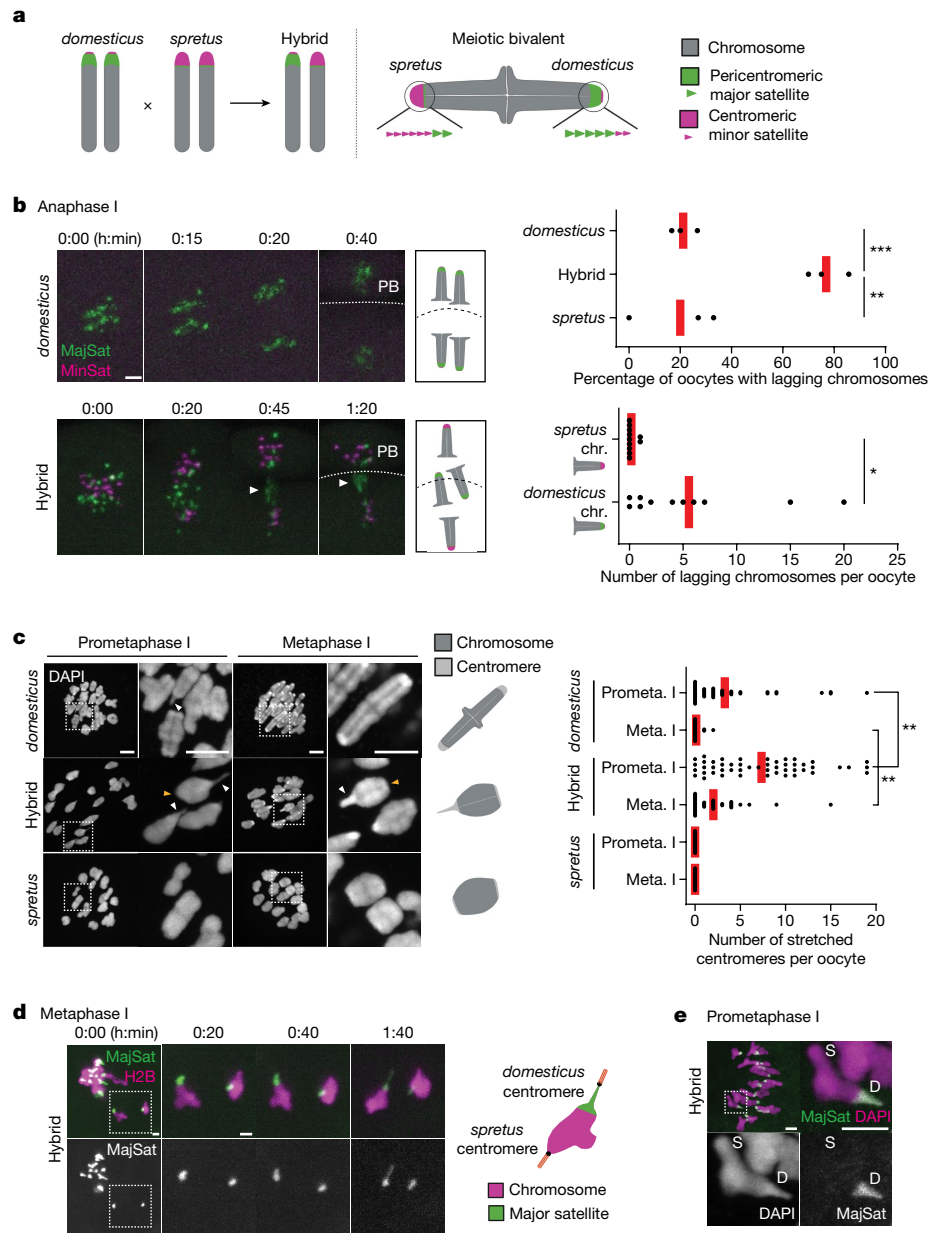


Fig. 1 | Species-specific chromosome mis-segregation driven by *domesticus* centromere stretching. **a**, Schematic of the hybrid mouse system to study hybrid incompatibility in female meiosis. **b**, Oocytes of *domesticus* and hybrid mice expressing TALE-mClover targeting major satellites (MajSat) and TALE-mRuby2 targeting *spretus* minor satellites (MinSat) were imaged live in anaphase I. MajSat and MinSat visualize *domesticus* and *spretus* centromeres, respectively. The white arrowheads show lagging chromosomes. The dashed lines show the oocyte cortex. PB, polar body. The anaphase lagging rate in *domesticus*, hybrid and *spretus* oocytes (top right; each dot represents an independent experiment) and the number of *spretus* and *domesticus* chromosomes lagging in hybrid oocytes (bottom right; each dot represents a single oocyte) were quantified. $n = 32, 21$ and 28 oocytes for *domesticus*, hybrid and *spretus*, respectively. Statistical analysis was performed using two-sided unpaired t -tests; $*P = 0.0125$, $**P = 0.007$, $***P = 0.0005$. **c**, Oocytes of *domesticus*, hybrid and *spretus* mice were fixed at prometaphase (prometa.) I or metaphase

(meta.) I and counterstained with DAPI. The white and orange arrowheads indicate stretched and compact centromeres, respectively. The number of stretched centromeres was quantified (prometaphase I: $n = 46, 49$ and 30 oocytes for *domesticus*, hybrid and *spretus*, respectively; metaphase I: $n = 39, 39$ and 22 oocytes for *domesticus*, hybrid and *spretus*, respectively). Each dot in the graph represents a single oocyte. Statistical analysis was performed using two-sided unpaired t -tests; $**P = 0.0002$. **d**, Hybrid oocytes expressing H2B-mCherry and MajSat were imaged live in metaphase I. **e**, Hybrid oocytes expressing MajSat were fixed at prometaphase I and counterstained with DAPI. Centromeres of *domesticus* (D) and *spretus* (S) are indicated. The experiments in **d** and **e** were repeated independently twice with similar results. The images are maximum-intensity z projections showing all chromosomes or optical slices magnified to show individual chromosomes. The red lines show the mean. For **b–e**, scale bars, $5\ \mu\text{m}$. Schematics in **a–d** were created using BioRender.

(Fig. 1c and Extended Data Fig. 1b–d (hybrid)). Furthermore, centromeres in hybrid oocytes were stretched even in metaphase I (Fig. 1c (hybrid)). Centromere stretching was always observed on just one side of the meiotic bivalent in hybrid oocytes, implying a species-specific

stretching of centromeres. Visualizing *domesticus* centromeres with a major satellite TALE construct in both fixed and live cells revealed that it was major satellites at *domesticus* centromeres that were stretching in hybrid oocytes (Fig. 1d,e). Stretched *domesticus* centromeres

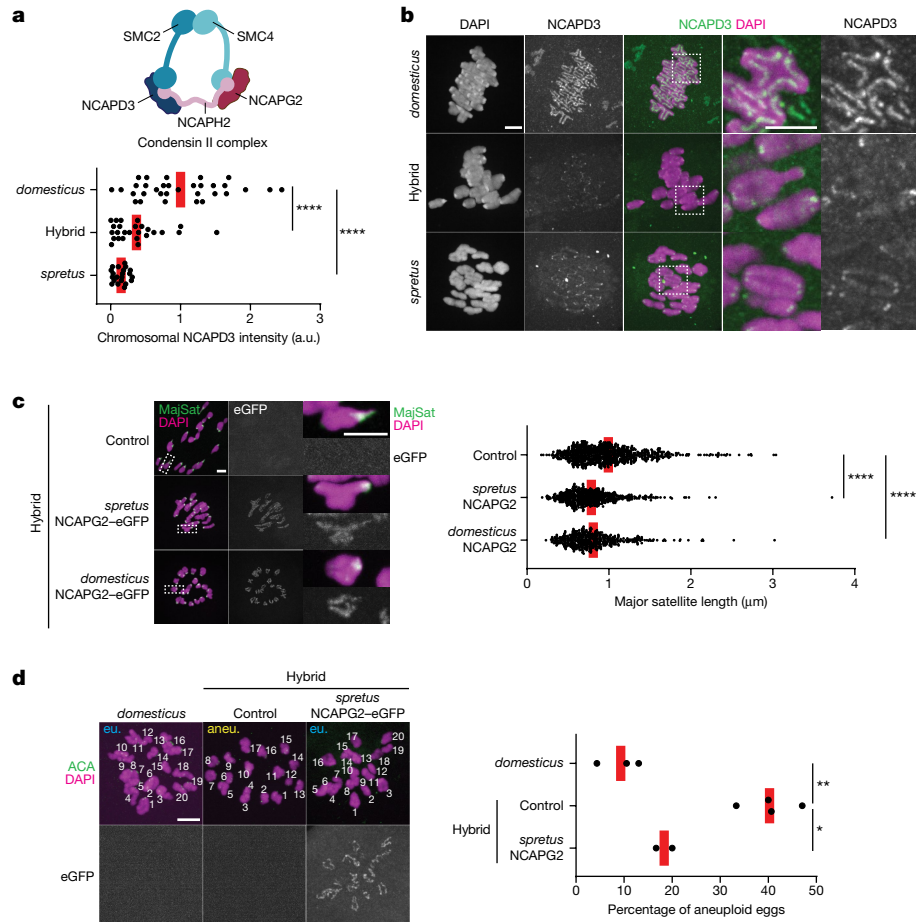


Fig. 2 | Condensin II dysfunction in hybrid oocytes causes egg aneuploidy. **a**, Schematic of the condensin II complex. **b**, Oocytes of *domesticus*, hybrid and *spretus* mice were fixed at metaphase I and stained for NCAPD3. NCAPD3 intensities on the chromosomes were quantified; each dot in the graph represents a single oocyte. $n = 32, 26$ and 21 oocytes for *domesticus*, hybrid and *spretus*, respectively. Statistical analysis was performed using two-sided unpaired t -tests; *** $P < 0.0001$. a.u., arbitrary units. **c**, Hybrid oocytes expressing NCAPG2-eGFP derived from *domesticus* or *spretus* were fixed at prometaphase I and stained for TOP2A (a major satellite marker; Extended Data Fig. 8b) and eGFP. The length of major satellites was quantified; each dot in the graph represents a single centromere. $n = 793, 606$ and 458 centromeres for control, *spretus* NCAPG2-eGFP and *domesticus* NCAPG2-eGFP, respectively.

Statistical analysis was performed using two-sided unpaired t -tests; *** $P < 0.0001$. **d**, Oocytes of *domesticus* and hybrid mice expressing *spretus* NCAPG2-eGFP were matured to metaphase II, fixed and stained for ACA (kinetochore) to perform the in situ chromosome counting assay. The aneuploid (aneu.) egg rate was quantified; each dot in the graph represents an independent experiment. eu., euploid. $n = 56, 66$ and 21 cells for *domesticus*, hybrid control and hybrid + *spretus* NCAPG2-eGFP, respectively. Statistical analysis was performed using two-sided unpaired t -tests; * $P = 0.0072$, ** $P = 0.0006$. The red lines show the mean. The images are maximum-intensity z projections showing all chromosomes or optical slices showing individual chromosomes. For **b–d**, scale bars, $5 \mu\text{m}$. The schematic in **a** was created using BioRender.

were more prone to spindle misattachments compared with *spretus* centromeres (Extended Data Fig. 1e), explaining why *domesticus* chromosomes preferentially mis-segregate in anaphase I (Fig. 1b). These results suggest that hybrid oocytes have chromosome condensation defects, especially impacting the *domesticus* centromere structure, leading to their species-specific mis-segregation. This observation raises the two fundamental questions of (1) why hybrid oocytes have overall chromosome condensation defects; and (2) why major satellites are most affected.

Condensin II dysfunction in hybrids

The condensin complex is a major factor in forming the rigid chromosome structure in mitosis and meiosis⁷. Many species have two condensin complexes—condensin I and II. Condensin I is cytoplasmic during interphase and gains access to the chromatin after nuclear envelope breakdown (NEBD)²⁴. By contrast, condensin II is enriched in the nucleus throughout the cell cycle and starts reorganizing the

chromatin in S phase to prepare for the segregation in M phase^{25–27}. Typically, condensin I has critical roles in mitosis, whereas condensin II has a major role in meiosis^{24,28,29}. The chromosomes are morphologically different between *domesticus* and hybrid oocytes (Fig. 1c and Extended Data Fig. 1b–d), suggesting that condensin is regulated differently between *domesticus* and hybrid oocytes. As the chromosome condensation defects and centromere stretching in hybrid oocytes phenocopied the depletion of functional condensin II complex in *domesticus* oocytes^{28,29} (Fig. 2a), we hypothesized that condensin II is misregulated in hybrid oocytes. To test this hypothesis, we analysed the localization of the condensin-II-specific subunit NCAPD3²⁸ in hybrid oocytes and found that condensin II was significantly reduced on the chromosome, including pericentromeric major satellites, while the kinetochore population was similar across all genotypes (Fig. 2b and Extended Data Fig. 2a,b).

Among hybrid oocytes, we noticed a variation in the condensin II abundance on the chromosome, which negatively correlated with the number of stretched centromeres per oocyte (Extended Data

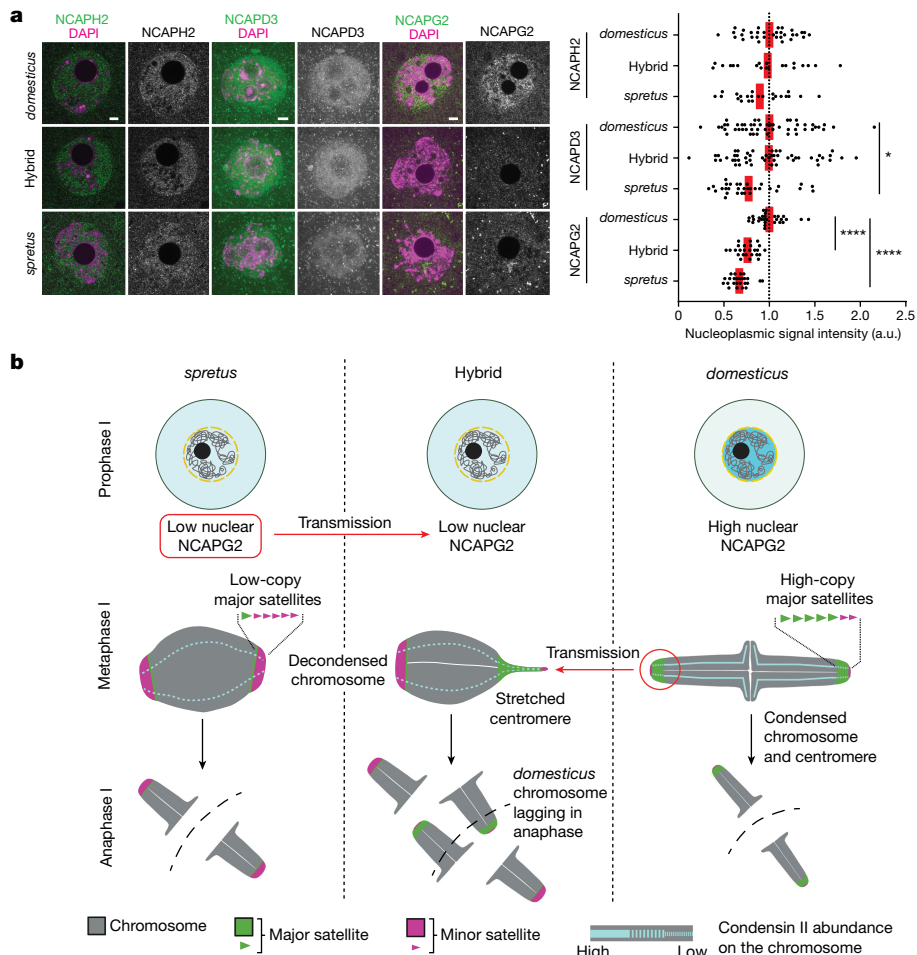


Fig. 3 | Species divergence in condensin regulation and centromere organization creates a reproductive isolating barrier. a, Oocytes of *domesticus*, hybrid and *spretus* mice were fixed at prophase I and stained for condensin II subunits. Their intensities in the nucleus were quantified; each dot in the graph represents a single oocyte. NCAPH2: $n = 32, 20; NCAPD3: $n = 50, 50; and NCAPG2: $n = 29, 25 oocytes for *domesticus*, hybrid and *spretus*, respectively. Statistical analysis was performed using two-sided unpaired *t*-tests; $*P = 0.0058$, $****P < 0.0001$. The red lines show the mean. Nuclear NCAPG2 was reduced both in *spretus* and hybrid oocytes, whereas NCAPD3 was reduced in *spretus* but not in hybrid oocytes. Images are optical slices showing the nucleus. Scale bars, 5 μm . **b,** Model of hybrid incompatibility$$$

reducing female fertility in *domesticus* \times *spretus* hybrid mice. Nuclear NCAPG2 levels are higher in *domesticus* and lower in *spretus*, which dictates the abundance of condensin II on metaphase chromosomes. Chromosomes in *domesticus* oocytes load higher levels of condensin II to condense major satellites, which is the chromosome region that is prone to stretching. By contrast, *spretus* oocytes enrich significantly less condensin II on the chromosome, but this low abundance is sufficient to condense their centromeres, which have very few major satellites. Hybrid oocytes inherited the low condensin II trait from *spretus* and the high major satellite copy number from *domesticus*, and this combination drives centromere stretching, causing meiotic failures. The schematic in **b** was created using BioRender.

Fig. 2c). Moreover, reducing the condensin II abundance further in hybrid oocytes by partially depleting the condensin-II-specific subunit NCAPH2 enhanced centromere stretching (Extended Data Fig. 2d). These results collectively suggest that the distinct chromosome morphology and centromere stretching in hybrid oocytes are due to their reduced condensin II abundance on the chromosome. In mouse oocytes lacking condensin II, condensin I staining is weaker on the chromosome axis possibly due to the swollen nature of chromatids²⁹. Consistent with the previous study, condensin I signals were reduced on the chromosome in hybrid oocytes (Extended Data Fig. 3a).

In contrast to oocyte cells, condensin II was not reduced in mitotic cells isolated from hybrid mice (Extended Data Fig. 3b). This difference could be attributed to the distinct activity profiles of CDK1, which facilitates the chromosome–condensin II interaction³⁰, between mitosis and female meiosis^{31–33} (Discussion).

If the reduced condensin II levels on the chromosome are indeed the cause of condensation defects and centromere stretching in hybrid oocytes, then overexpression of condensin II subunits may rescue this phenotype. To test this hypothesis, we overexpressed each of

the condensin-II-specific subunits, NCAPG2, NCAPD3 and NCAPH2, in hybrid oocytes (Fig. 2c and Extended Data Fig. 4). Among these subunits, overexpression of NCAPG2-eGFP efficiently rescued centromere stretching by increasing the condensin II abundance on the chromosome (Fig. 2c and Extended Data Fig. 7a). Importantly, overexpressing NCAPG2-eGFP also rescued egg aneuploidy in the hybrid (Fig. 2d), demonstrating that condensin misregulation is one of the major hybrid incompatibilities affecting female fertility and maintaining the reproductive isolation between these species. As *domesticus* and *spretus* NCAPG2-eGFP showed similar localization patterns and rescue efficiencies (Fig. 2c and Extended Data Fig. 7b), their amino acid sequence divergence seems not to be part of the hybrid incompatibility in chromosome condensation (Extended Data Fig. 5a).

Reduced NCAPG2 in the nucleus

Rescuing condensation defects and aneuploidy by overexpressing a single condensin II subunit implies that NCAPG2 may be a rate-limiting

factor to form a functional condensin II complex in this hybrid system. To test this idea, we examined the localization of condensin II subunits in late prophase I, during which they have the opportunity to interact with the chromatin in the nucleus before NEBD^{27,28} (Fig. 3a and Extended Data Fig. 6a,b (*domesticus*)). We found that NCAPG2 was significantly less enriched in the nucleus in hybrid oocytes compared with in *domesticus* oocytes, whereas all other subunits were normally enriched in the nucleus (Fig. 3a and Extended Data Fig. 6a,b). This specific reduction in NCAPG2 from hybrid oocyte nuclei can explain why the NCAPG2 overexpression efficiently rescued centromere stretching and egg aneuploidy. We also confirmed that overexpressed NCAPG2 localizes to the nucleus in hybrid oocytes (Extended Data Fig. 7b,c). As total NCAPG2 protein levels were similar between *domesticus* and hybrid oocytes (Extended Data Fig. 6c), the nuclear–cytoplasmic transport of NCAPG2 could be differentially regulated between the two genotypes, reducing its nuclear localization specifically in hybrid oocytes. To test the importance of nuclear NCAPG2 enrichment for the localization of condensin II on metaphase chromosomes, we overexpressed the NCAPG2 construct fused to nuclear export signals (NCAPG2–NES–eGFP). NCAPG2–NES–eGFP did not enrich in the nucleus and localized less on metaphase chromosomes compared with NCAPG2–eGFP (Extended Data Fig. 7b–d). Importantly, NCAPG2–NES–eGFP was less efficient in rescuing centromere stretching compared with NCAPG2–eGFP (Extended Data Fig. 7d), demonstrating the importance of nuclear enrichment of NCAPG2 for timely chromosome condensation in metaphase.

Notably, pure *spretus* oocytes also showed reduced NCAPG2 levels in prophase I nuclei and low condensin II levels on metaphase chromosomes, mimicking the localization patterns in hybrid oocytes (Figs. 2b and 3a and Extended Data Figs. 2a and 6b). As a consequence, chromosomes in *spretus* oocytes were significantly shorter and wider compared with those in *domesticus* oocytes (Fig. 1c and Extended Data Fig. 1b–d). The similarity in condensin dynamics between hybrid and *spretus* oocytes implies that hybrids inherited the reduced condensin II trait from *spretus*, eventually leading to stretching *domesticus* centromeres in hybrid oocytes. Importantly, even though pure *spretus* oocytes have very low chromosomal condensin II levels resulting in less-condensed chromosomes, their centromeres were not stretched and chromosomes segregated normally (Fig. 1b,c). This could be explained by *spretus* centromeres having very few major satellites, which is the chromosome region prone to stretching (Fig. 3b). By contrast, *domesticus* oocytes enrich higher levels of condensin II on the chromosome to prevent major satellite stretching (Fig. 2b and Extended Data Fig. 2b). These results demonstrate a substantial species divergence in the essential chromosome condensation process between *domesticus* and *spretus*. As a result, hybrid oocytes inherit the reduced condensin II trait from *spretus* and major satellites from *domesticus*, and we propose that this combination is what causes major satellites to stretch, leading to species-specific chromosome mis-segregation and reduced fertility.

Major satellites reduce condensin II further

The reduced condensin II abundance in hybrid oocytes addressed the first question of why hybrid oocytes have overall chromosome condensation defects. However, the second question, of why major satellites are most affected, remains unresolved. We addressed this question by analysing the condensin II localization pattern within the chromosome in hybrid oocytes. This analysis revealed that the major satellite region enriched significantly less condensin II compared with the rest of the chromosome (Fig. 4a and Extended Data Fig. 8a). As chromosomal condensin II levels are already lower in hybrid oocytes (Fig. 2b), this further reduction at major satellites imposes an extra challenge to condense this region, explaining why major satellites are prone to stretching (Fig. 1d,e). To understand why major satellites

enrich less condensin II, we focused on factors that highly enrich at the major satellite region. One such factor is topoisomerase IIA (TOP2A), which is another major player in chromosome structure^{28,34} (Extended Data Fig. 8b). We found that centromeric TOP2A levels were higher at stretched centromeres compared with at unstretched ones in hybrid oocytes (Fig. 4b and Extended Data Fig. 8c). Furthermore, the major satellite length was significantly longer when over-expressing eGFP–TOP2A (Extended Data Fig. 8d). These observations raised the possibility that major satellites reduce condensin II levels through TOP2A. To test whether the enrichment of TOP2A is sufficient to induce centromere stretching by reducing condensin II abundance, we ectopically enriched TOP2A to *spretus* centromeres where TOP2A levels are usually very low (Fig. 4c and Extended Data Fig. 8b). To target TOP2A to *spretus* centromeres in hybrid oocytes, we fused TOP2A to a TALE construct specific to *spretus* minor satellites (MinSat–TOP2A)⁴ (Fig. 4c and Extended Data Fig. 9a). The ectopic TOP2A targeting significantly reduced condensin II levels at *spretus* centromeres and induced their stretching in a catalytic-activity-dependent manner (Fig. 4d,e and Extended Data Fig. 9b,c). These results suggest that major satellites reduce condensin II levels possibly through TOP2A, leading to their stretching in hybrid oocytes in which chromosomal condensin II levels are lower to begin with (Extended Data Fig. 9d).

As a complementary approach to the ectopic TOP2A targeting, we sought to develop a strategy to reduce TOP2A at major satellites to test whether it is sufficient to rescue centromere stretching. Earlier studies in mouse oocytes have shown that the global inhibition of TOP2A disrupts the overall chromosome structure^{35,36}, making it technically challenging to analyse centromere stretching. This technical challenge prompted us to develop an approach to reduce TOP2A specifically at major satellites to maintain the overall chromosome structure. We found that overexpression of the MajSat TALE construct reduced TOP2A abundance specifically at major satellites while maintaining its axis localization and the overall chromosome structure (Extended Data Fig. 10a). Importantly, this manipulation rescued centromere stretching (Extended Data Fig. 10a), possibly through increasing condensin II levels at major satellites (Extended Data Fig. 10b). Together, these results suggest that the combination of less NCAPG2 in the nucleus, which reduces overall chromosomal condensin II levels, and expanded major satellites, which reduces condensin II further through TOP2A, leads to centromere stretching and mis-segregation in hybrid oocytes (Fig. 3b and Extended Data Fig. 9d).

Condensin II levels in other species

We next extended our condensin analysis to include additional mouse species from the *Mus* genus (Fig. 5a). By comparing oocytes from four different species (*domesticus*, *Mus musculus musculus* (hereafter, *musculus*), *spretus* and *Mus spicilegus* (hereafter *spicilegus*), we found a significant species divergence in their condensin II abundance on the chromosome (Fig. 5b). Notably, the species divergence in condensin II levels correlated with their reported major satellite copy numbers³⁷ (Fig. 5a,b and Extended Data Fig. 6e), implying that major satellite expansions lead to higher condensin II levels on metaphase chromosomes to properly compact centromeres. Analysing centromeric TOP2A levels revealed that there was no species with a combination of higher centromeric TOP2A and lower chromosomal condensin II levels (Fig. 5b,c), which would lead to centromere stretching and chromosome mis-segregation as in *domesticus* × *spretus* hybrid oocytes (Fig. 1b,d). Species with higher chromosomal condensin II levels (*musculus* and *domesticus*) also showed higher nuclear NCAPG2 levels (Extended Data Figs. 5c and 6d), consistent with the model that the nuclear NCAPG2 enrichment contributes to localizing condensin II on metaphase chromosomes (Fig. 3b). However, the variation in chromosomal condensin II levels cannot be fully explained by nuclear NCAPG2 levels. For example,

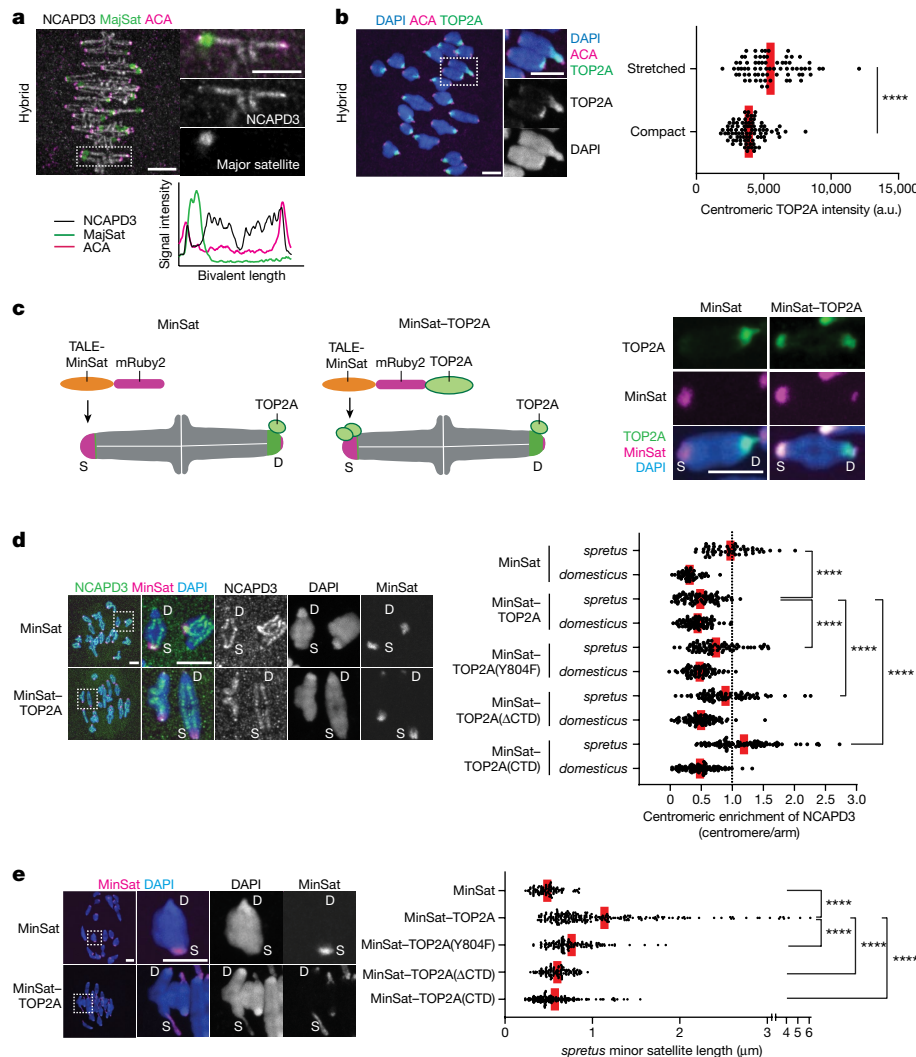


Fig. 4 | Major satellites reduce condensin II further through TOP2A. **a**, Hybrid oocytes expressing MajSat were fixed at metaphase I and stained for NCAPD3 and ACA. The graph is line scans of relative signal intensities across the chromosome length. This experiment was repeated independently twice with similar results. **b**, Hybrid oocytes were fixed at prometaphase I and stained for TOP2A and ACA. Chromosomes were categorized into two groups on the basis of *domesticus* centromere stretching, and their TOP2A signal intensities at *domesticus* centromeres were quantified. $n = 87$ and 72 centromeres for compact and stretched, respectively. Statistical analysis was performed using two-sided unpaired t -tests; *** $P < 0.0001$. **c**, Schematic of the strategy to target TOP2A to *spretus* minor satellites. Hybrid oocytes expressing MinSat or MinSat-TOP2A were fixed at prometaphase I and stained for TOP2A (Extended Data Fig. 9a). This experiment was repeated independently twice with similar results. **d**, **e**, Hybrid oocytes expressing MinSat, MinSat-TOP2A,

MinSat-TOP2A(Y804F), MinSat-TOP2A(Δ CTD) or MinSat-TOP2A(CTD) were either fixed at metaphase I and stained for NCAPD3 (d) or fixed at prometaphase I and counterstained with DAPI (e). The graphs show centromeric enrichment of NCAPD3, calculated as the centromeric signal (minor satellite signals for *spretus* centromeres and major satellite signals for *domesticus* centromeres) divided by the chromosome arm signal for each half-bivalent (d, $n = 65, 74, 71, 83$ and 106 centromeres for MinSat, MinSat-TOP2A, MinSat-TOP2A(Y804F), MinSat-TOP2A(Δ CTD) and MinSat-TOP2A(CTD), respectively) or the length of *spretus* minor satellites (e, $n = 97, 223, 134, 118$ and 197 centromeres for MinSat, MinSat-TOP2A, MinSat-TOP2A(Y804F), MinSat-TOP2A(Δ CTD) and MinSat-TOP2A(CTD), respectively). Statistical analysis was performed using two-sided unpaired t -tests; *** $P < 0.0001$. Each dot in the graph represents a single centromere. The red lines show the mean. For a–e, scale bars, 5 μ m. The schematic in c was created using BioRender.

spicilegus oocytes have very low nuclear NCAPG2 levels with modest condensin II enrichment on metaphase chromosomes, suggesting that other condensin II regulators also modulate condensin II levels on metaphase chromosomes^{38,39}.

Finally, we generated two additional hybrid mice (*musculus* × *spretus* and *domesticus* × *spicilegus*) to test whether we observe centromere stretching (Fig. 5d). *musculus* × *spretus* hybrid oocytes showed significantly lower condensin II abundance on the chromosome and frequent centromere stretching. By contrast, *domesticus* × *spicilegus* hybrid oocytes showed higher condensin II abundance on the chromosome and very few stretched centromeres. These results are consistent with our model that the combination of expanded major satellites and the

low condensin II abundance drives centromere stretching, establishing a reproductive isolating barrier.

Discussion

Here we provide cell biological insights into hybrid incompatibility in female meiosis, revealing that species divergence in centromere organization and condensin regulation drives meiotic failures, creating a reproductive isolating barrier (Fig. 3b). Hybrid *domesticus* × *spretus* mice also have male fertility issues mainly due to the defective chromosome pairing during meiotic prophase⁴⁰. Notably, a recent study

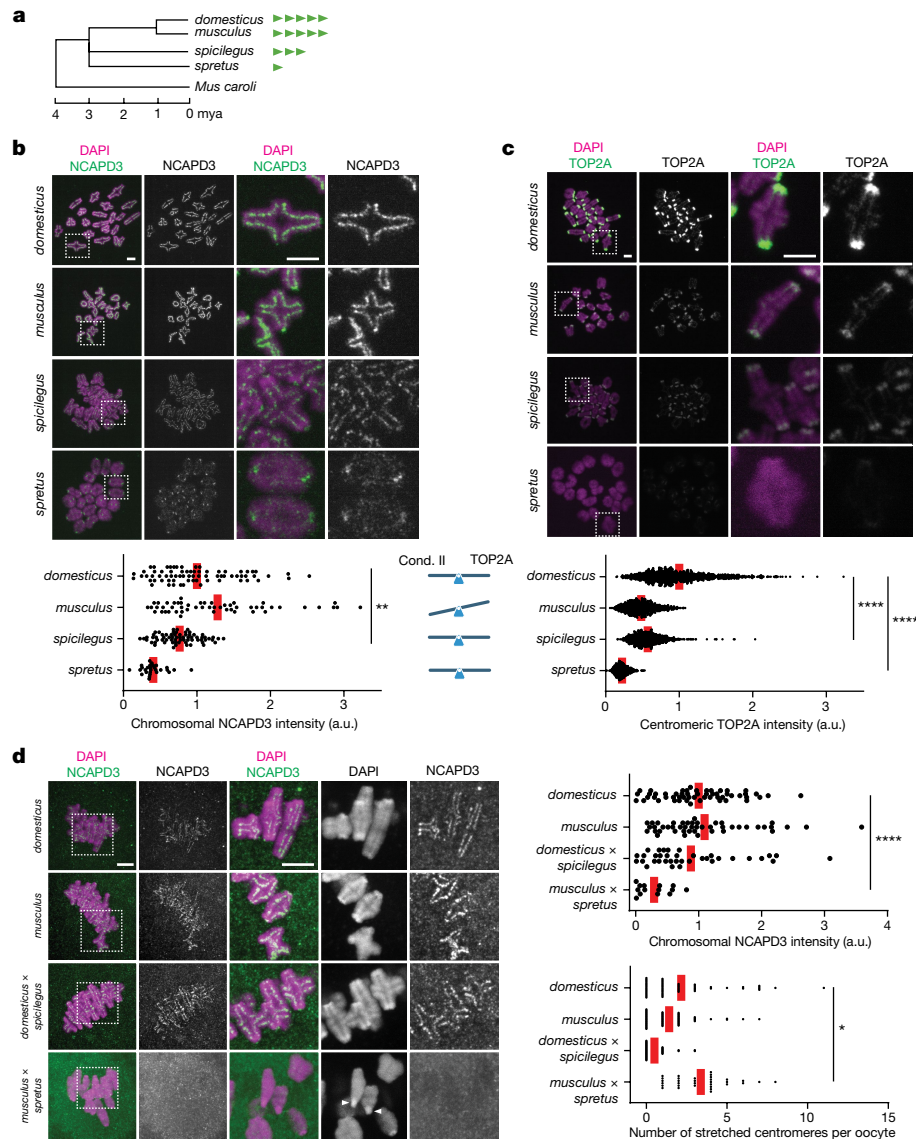


Fig. 5 | Condensin II regulation across the *Mus* genus. **a**, Phylogenetic tree of mouse species. The green arrowheads indicate relative major satellite copy numbers³⁷ (Extended Data Fig. 6e). mya, million years ago. **b,c**, Chromosome spreads were performed at metaphase I using *domesticus*, *musculus*, *spretus* and *spicilegus* oocytes and stained for NCAPD3 (**b**) or TOP2A (**c**). NCAPD3 intensities on chromosomes (**b**; $n = 71, 52, 68$ and 28 oocytes for *domesticus*, *musculus*, *spretus* and *spicilegus*, respectively; each dot in the graph represents a single oocyte) and centromeric TOP2A intensities (**c**; $n = 1,322, 819, 1,051$ and 639 centromeres for *domesticus*, *musculus*, *spretus* and *spicilegus*, respectively; each dot in the graph represents a single centromere) were quantified. Statistical analysis was performed using two-sided unpaired *t*-tests; ** $P = 0.0017$, **** $P < 0.0001$. The balance symbols indicate the relative abundance of condensin II (cond. II) and TOP2A within the species. There was no species with a combination of high TOP2A and low condensin II, which would stretch

centromeres. As the NCAPD3 amino acid sequences among these species are conserved, the observed species divergence in NCAPD3 levels is not due to different efficiencies in antibody recognition (Extended Data Fig. 5b). **d**, Oocytes of *domesticus*, *musculus*, *domesticus* × *spicilegus*, and *musculus* × *spretus* mice were fixed at metaphase I and stained for NCAPD3. The white arrowheads indicate stretched centromeres. NCAPD3 intensities on chromosomes ($n = 54, 46, 36$ and 14 oocytes for *domesticus*, *musculus*, *domesticus* × *spicilegus* and *musculus* × *spretus*, respectively) and the number of stretched centromeres ($n = 55, 60, 38$ and 32 oocytes for *domesticus*, *musculus*, *domesticus* × *spicilegus* and *musculus* × *spretus*, respectively) was quantified. Each dot in the graph represents a single oocyte. Statistical analysis was performed using two-sided unpaired *t*-tests; * $P = 0.0208$, **** $P < 0.0001$. The red lines show the mean. For **b–d**, scale bars, $5\ \mu\text{m}$. The schematic in **a–c** was created using BioRender.

showed that rescuing the pairing defects in male hybrids only partially restored their fertility, raising the possibility that other incompatibilities during chromosome segregation are at play, further reducing their fertility⁴¹.

Condensin II was reduced in hybrid oocytes but not in their somatic cells (Extended Data Fig. 3b), which explains why *domesticus* × *spretus* hybrids develop normally but have fertility issues⁴². The CDK1 activity, which facilitates the chromosome–condensin II association³⁰, could explain the difference between mitosis and female meiosis. The CDK1

activity is already very high after NEBD in mitosis and remains high until anaphase, whereas, in oocytes, it is lower in prometaphase I, gradually increases and eventually peaks just before anaphase I^{31–33}. This lower CDK1 activity in prometaphase I could impose an extra challenge to condense chromosomes in oocytes. Consistent with this idea, stretched centromeres were observed more frequently in pro-metaphase I (lower CDK1) compared with in metaphase I (higher CDK1) (Fig. 1c). It would be interesting to test whether the lower CDK1 activity in oocytes makes the nuclear enrichment of condensin II subunits

especially important for timely chromosome condensation in this cell division.

This study also raises the possibility that the condensin II abundance on metaphase chromosomes co-evolves with the major satellite copy number to prevent centromere stretching in oocytes (Fig. 5a,b). It is interesting to consider why several *Mus* genus mice carry large major satellite repeats in their genome, which make their pericentromeres more fragile by reducing condensin II. We think that there is an advantage to have expanded major satellite repeats. Indeed, multiple studies have reported that transcripts from major satellites regulate heterochromatin formation and embryo development in *domesticus*^{43,44}.

Our results suggest that major satellites reduce condensin II levels through TOP2A (Fig. 4). Although it remains unclear how TOP2A reduces condensin II, ectopic TOP2A-targeting experiments suggest that both TOP2A's catalytic activity and the C-terminal domain (CTD), which is critical to guide TOP2A to the chromosome axis, are important to reduce condensin II (Fig. 4d,e and Extended Data Fig. 9). Condensins drive DNA loop extrusion with their ATPase domains⁴⁵, and it is thought that they fall off from chromosomes when they cannot efficiently perform loop extrusion^{46,47}. One possible mechanism underlying the TOP2A-mediated reduction in condensin II is that high TOP2A enrichment induces substantial DNA intercatenation at major satellites⁴⁸, which restricts condensin-II-dependent loop extrusion, ultimately leading to a decrease in condensin II at this chromosome region. The major-satellite-specific depletion of TOP2A reduced sister chromatid catenation at major satellites and increased condensin II levels, supporting this model (Extended Data Fig. 10b). In addition to TOP2A inducing overcatenation, it is also possible that TOP2A indirectly modulates condensin II levels through other factors such as histone H1 and MCPH1 or by altering the nucleosome density^{38,39,49,50}. Future study would reveal the molecular basis underlying how the high TOP2A enrichment locally reduces condensin II.

Condensin II is implicated in centromere drive, whereby selfish centromeres preferentially segregate to the egg to increase their own transmission rate^{51,52}. On the basis of the original centromere drive theory, centromere DNA evolves rapidly to develop a strategy to bias its segregation to the egg. Evolution of condensin regulations, including how they interact with centromere satellites, could be a strategy of the genome to fight back against selfish centromeres to suppress their cheating^{8,53}. Thus, this reproductive isolating barrier could be a consequence of genetic conflict between selfish elements and the rest of the genome^{3,54}.

Online content

Any methods, additional references, Nature Portfolio reporting summaries, source data, extended data, supplementary information, acknowledgements, peer review information; details of author contributions and competing interests; and statements of data and code availability are available at <https://doi.org/10.1038/s41586-023-06700-6>.

- Coyne, J. A. & Orr, H. A. Speciation (Sinauer, 2004).
- Orr, H. A., Masly, J. P. & Presgraves, D. C. Speciation genes. *Curr. Opin. Genet. Dev.* **14**, 675–679 (2004).
- Johnson, N. A. Hybrid incompatibility genes: remnants of a genomic battlefield? *Trends Genet.* **26**, 317–325 (2010).
- Miyanari, Y., Ziegler-Birling, C. & Torres-Padilla, M.-E. Live visualization of chromatin dynamics with fluorescent TALEs. *Nat. Struct. Mol. Biol.* **20**, 1321–1324 (2013).
- Narayanswami, S. et al. Cytological and molecular characterization of centromeres in *Mus domesticus* and *Mus spretus*. *Mamm. Genome* **2**, 186–194 (1992).
- Wong, A. K. C., Biddle, F. G. & Rattner, J. B. The chromosomal distribution of the major and minor satellite is not conserved in the genus *Mus*. *Chromosoma* **99**, 190–195 (1990).
- Hirano, T. Condensin-based chromosome organization from bacteria to vertebrates. *Cell* **164**, 847–857 (2016).
- Hoencamp, C. et al. 3D genomics across the tree of life reveals condensin II as a determinant of architecture type. *Science* **372**, 984–989 (2021).
- Mihola, O., Trachulec, Z., Vlcek, C., Schimenti, J. C. & Forejt, J. A mouse speciation gene encodes a meiotic histone H3 methyltransferase. *Science* **323**, 373–375 (2009).
- Brideau, N. J. et al. Two Dobzhansky-Muller genes interact to cause hybrid lethality in *Drosophila*. *Science* **314**, 1292–1295 (2006).
- Phadnis, N. et al. An essential cell cycle regulation gene causes hybrid inviability in *Drosophila*. *Science* **350**, 1552–1555 (2015).
- Suzuki, T. A. & Nachman, M. W. Speciation and reduced hybrid female fertility in house mice. *Evolution* **69**, 2468–2481 (2015).
- Sturtevant, A. H. Genetic studies on *Drosophila simulans*. I. Introduction. Hybrids with *Drosophila melanogaster*. *Genetics* **5**, 488–500 (1920).
- Chiang, T., Schultz, R. M. & Lampson, M. A. Meiotic origins of maternal age-related aneuploidy. *Biol. Reprod.* **86**, 1–7 (2012).
- Kitajima, T. S. Mechanisms of kinetochore-microtubule attachment errors in mammalian oocytes. *Dev. Growth Differ.* **60**, 33–43 (2018).
- Nagaoka, S. I., Hassold, T. J. & Hunt, P. A. Human aneuploidy: mechanisms and new insights into an age-old problem. *Nat. Rev. Genet.* **13**, 493–504 (2012).
- Thomas, C., Cavazza, T. & Schuh, M. Aneuploidy in human eggs: contributions of the meiotic spindle. *Biochem. Soc. Trans.* **49**, 107–118 (2021).
- Sebestova, J., Danylevska, A., Novakova, L., Kubelka, M. & Anger, M. Lack of response to unaligned chromosomes in mammalian female gametes. *Cell Cycle* **11**, 3011–3018 (2012).
- Asakawa, T., Ishikawa, M., Shimizu, T. & Dukelow, W. R. The chromosomal normality of in vitro-fertilized rabbit oocytes. *Biol. Reprod.* **38**, 292–295 (1988).
- Nicodemo, D. et al. Frequency of aneuploidy in in vitro-matured MII oocytes and corresponding first polar bodies in two dairy cattle (*Bos taurus*) breeds as determined by dual-color fluorescent in situ hybridization. *Theriogenology* **73**, 523–529 (2010).
- Vozdová, M. et al. Frequency of aneuploidy in pig oocytes matured in vitro and of the corresponding first polar bodies detected by fluorescent in situ hybridization. *Theriogenology* **56**, 771–776 (2001).
- Koehler, K. E., Schrump, S. E., Cherry, J. P., Hassold, T. J. & Hunt, P. A. Near-human aneuploidy levels in female mice with homeologous chromosomes. *Curr. Biol.* **16**, R579–R580 (2006).
- Reichmann, J. et al. Dual-spindle formation in zygotes keeps parental genomes apart in early mammalian embryos. *Science* **361**, 189–193 (2018).
- Hirota, T., Gerlich, D., Koch, B., Ellenberg, J. & Peters, J.-M. Distinct functions of condensin I and II in mitotic chromosome assembly. *J. Cell Sci.* **117**, 6435–6445 (2004).
- Ono, T. et al. Differential contributions of condensin I and condensin II to mitotic chromosome architecture in vertebrate cells. *Cell* **115**, 109–121 (2003).
- Ono, T., Fang, Y., Spector, D. L. & Hirano, T. Spatial and temporal regulation of condensins I and II in mitotic chromosome assembly in human cells. *Mol. Biol. Cell* **15**, 3296–3308 (2004).
- Ono, T., Yamashita, D. & Hirano, T. Condensin II initiates sister chromatid resolution during S phase. *J. Cell Biol.* **200**, 429–441 (2013).
- Lee, J., Ogushi, S., Saitou, M. & Hirano, T. Condensins I and II are essential for construction of bivalent chromosomes in mouse oocytes. *Mol. Biol. Cell* **22**, 3465–3477 (2011).
- Hougaard, M. et al. Condensin confers the longitudinal rigidity of chromosomes. *Nat. Cell Biol.* **17**, 771–781 (2015).
- Abe, S. et al. The initial phase of chromosome condensation requires Cdk1-mediated phosphorylation of the CAP-D3 subunit of condensin II. *Genes Dev.* **25**, 863–874 (2011).
- Choi, T. et al. Activation of p34^{cdk2} protein kinase activity in meiotic and mitotic cell cycles in mouse oocytes and embryos. *Development* **113**, 789–795 (1991).
- Davydenko, O., Schultz, R. M. & Lampson, M. A. Increased CDK1 activity determines the timing of kinetochore-microtubule attachments in meiosis I. *J. Cell Biol.* **202**, 221–229 (2013).
- Yoshida, S., Kaido, M. & Kitajima, T. S. Inherent instability of correct kinetochore-microtubule attachments during meiosis I in oocytes. *Dev. Cell* **33**, 589–602 (2015).
- Pommier, Y., Nussenzeig, A., Takeda, S. & Austin, C. Human topoisomerases and their roles in genome stability and organization. *Nat. Rev. Mol. Cell Biol.* **23**, 407–427 (2022).
- Zhang, J. et al. Topoisomerase II dysfunction causes metaphase I arrest by activating Aurora B, SAC and MPF and prevents PB1 abscission in mouse oocytes. *Biol. Reprod.* **106**, 900–909 (2022).
- Li, X.-M. et al. DNA topoisomerase II is dispensable for oocyte meiotic resumption but is essential for meiotic chromosome condensation and separation in mice. *Biol. Reprod.* **89**, 118 (2013).
- Arora, U. P., Charlebois, C., Lawal, R. A. & Dumont, B. L. Population and subspecies diversity at mouse centromere satellites. *BMC Genom.* **22**, 279 (2021).
- Yamashita, D. et al. MCPH1 regulates chromosome condensation and shaping as a composite modulator of condensin II. *J. Cell Biol.* **194**, 841–854 (2011).
- Hougaard, M. et al. MCPH1 inhibits condensin II during interphase by regulating its SMC2-kleisin interface. *eLife* **10**, e73348 (2021).
- Hale, D. W., Washburn, L. L. & Eicher, E. M. Meiotic abnormalities in hybrid mice of the C57BL/6J x *Mus spretus* cross suggest a cytogenetic basis for Haldane's rule of hybrid sterility. *Cytogenet. Cell Genet.* **63**, 221–234 (1993).
- Davies, B. et al. Altering the binding properties of PRDM9 partially restores fertility across the species boundary. *Mol. Biol. Evol.* **38**, 5555–5562 (2021).
- Dejager, L., Libert, C. & Montagutelli, X. Thirty years of *Mus spretus*: a promising future. *Trends Genet.* **25**, 234–241 (2009).
- Probst, A. V. et al. A strand-specific burst in transcription of pericentric satellites is required for chromocenter formation and early mouse development. *Dev. Cell* **19**, 625–638 (2010).
- Burton, A. et al. Heterochromatin establishment during early mammalian development is regulated by pericentromeric RNA and characterized by non-repressive H3K9me3. *Nat. Cell Biol.* **22**, 767–778 (2020).
- Terakawa, T. et al. The condensin complex is a mechanochemical motor that translocates along DNA. *Science* **358**, 672–676 (2017).
- Kong, M. et al. Human condensin I and II drive extensive ATP-dependent compaction of nucleosome-bound DNA. *Mol. Cell* **79**, 99–114 (2020).

47. Kinoshita, K., Kobayashi, T. J. & Hirano, T. Balancing acts of two HEAT subunits of condensin I support dynamic assembly of chromosome axes. *Dev. Cell* **33**, 94–106 (2015).
48. Hsieh, T. Knotting of the circular duplex DNA by type II DNA topoisomerase from *Drosophila melanogaster*. *J. Biol. Chem.* **258**, 8413–8420 (1983).
49. Haase, J., Chen, R., Bonner, M. K., Jenkins, L. M. M. & Kelly, A. E. The TFIIH complex is required to establish and maintain mitotic chromosome structure. *eLife* <https://doi.org/10.1101/467569> (2022).
50. Choppakatla, P. et al. Linker histone H1.8 inhibits chromatin binding of condensins and DNA topoisomerase II to tune chromosome length and individualization. *eLife* **10**, e68918 (2021).
51. Akera, T., Trimm, E. & Lampson, M. A. Molecular strategies of meiotic cheating by selfish centromeres. *Cell* **178**, 1132–1144 (2019).
52. Henikoff, S., Ahmad, K. & Malik, H. S. The centromere paradox: stable inheritance with rapidly evolving DNA. *Science* **293**, 1098–1102 (2001).
53. King, T. D. et al. Recurrent losses and rapid evolution of the condensin II complex in insects. *Mol. Biol. Evol.* **36**, 2195–2204 (2019).
54. Phadnis, N. & Orr, H. A. A single gene causes both male sterility and segregation distortion in *Drosophila* hybrids. *Science* **323**, 376–379 (2009).

Publisher's note Springer Nature remains neutral with regard to jurisdictional claims in published maps and institutional affiliations.

© This is a U.S. Government work and not under copyright protection in the US; foreign copyright protection may apply 2023

Article

Methods

Mouse strains

Mouse strains were purchased from Envigo (NSA, 033 corresponds to CF-1, *M. m. domesticus*), Jackson Laboratory (C57BL/6J, 000664, *M. m. domesticus*; PWD/PhJ, 004660, *M. m. musculus*) and RIKEN BioResource Research Center (SPR2, RBRC00208, *M. spretus*; ZBN/Ms, RBRC00661, *M. spicilegus*). CF-1 and C57BL/6J mice share the same centromere organization⁵⁵ and have complementary advantages as *M. m. domesticus* strains: CF-1 is an outbred strain with a significantly higher oocyte yield and C57BL/6J is an inbred strain that efficiently produces hybrid offspring with SPR2. *M. m. domesticus* C57BL/6J female mice were crossed to *M. spretus* SPR2 or *M. spicilegus* ZBN/Ms male mice to generate F₁ hybrids, because the other direction is significantly less efficient in producing offspring. Similarly, *M. m. musculus* PWD/PhJ female mice were crossed to *M. spretus* SPR2 male mice to generate F₁ hybrids, owing to the technical difficulty to cross in the other direction. Mice were housed in an animal facility under a 12 h–12 h light–dark cycle at room temperature with minimal disturbance with a range of 30–70% humidity depending on the season. All animal experiments were approved by the Animal Care and Use Committee (National Institutes of Health Animal Study Proposal: H-0327) and were consistent with the National Institutes of Health guidelines.

Mouse oocyte collection and culture

Germinal-vesicle-intact oocytes were collected from female mice (aged 6–12 weeks) in the M2 medium (Sigma-Aldrich, M7167) supplemented with 5 μM milrinone (Sigma-Aldrich, 475840) to prevent meiotic resumption. After the oocyte collection, oocytes were transferred to the M16 medium (Millipore, M7292) containing 5 μM milrinone covered with paraffin oil (Nacalai, NC1506764) and incubated at 37 °C in a humidified atmosphere of 5% CO₂ in air. To induce meiotic resumption, milrinone was washed out, and oocytes that did not undergo NEBD within 1.5 h after the milrinone washout were removed from the culture. For the in situ chromosome counting assay, oocytes were matured for 13 h after NEBD and subsequently treated with 100 μM monastrol (Millipore, 475879) in the organ culture dish (Falcon, 353037) for 2 h 15 min before fixation⁵⁶.

Plasmid construction and mutagenesis

Constructs to express NCAPG2, NCAPD3 and NCAPH2 were created by amplifying their coding sequences from a *M. m. domesticus* or *M. spretus* cDNA library by PCR and subcloning them into the plasmid in vitro transcription (pIVT) vector with an N-terminal eGFP for NCAPD3 and a C-terminal eGFP for NCAPG2 and NCAPH2⁵⁷. The following primers were used for the PCR amplifications: 5'-TCA AGCTTGATGCCTGCAGATGGAAAAACGTGAGGCGTTCA-3' and 5'-TGCTCACCATTCAGATGGATTCAAATTCTCCAAAGT-3' (*Ncapg2*); 5'-TGCATGGAGGATGTGGAGGTGCGCTTGCTCAC-3' and 5'-CC ATTCTAGAGTCGACAGGCTGGGCATGGATGG-3' (*Ncaph2*); and 5'-GCTGTACAAGGTGCGACATGGCGTGCAGGATCTTCAAGGG-3' (*Ncapd3*). The NCAPG2-NES construct was created by amplifying the 3×NES sequence (the original duplex oligonucleotide was synthesized by Integrated DNA Technologies) using the following primers: 5'-TCTGAATCCATCTAGAACATGGAGGAACCTTTCACAGGCC-3' and 5'-TGCTCACCATCTAGAAAGTTCGAGCTCCTCCAGTTTC-3', which was inserted between the NCAPG2 and eGFP sequences. Constructs to target TOP2A to *spretus* minor satellites were created by amplifying the *Top2a* coding sequence from a *M. m. domesticus* cDNA library by PCR and subcloning it into the TALE-MinSat vector (Addgene, 47879). The following primers were used for the PCR amplification of *Top2a*: 5'-ATGGACGAGCTGTACAAGATGGAGTTGTCACCGCTGCA-3' and 5'-GGTGCCATATGTACATCAGAAGAGTCGTCATCG-3'. To create the catalytic-dead TOP2A mutant construct, the active site tyrosine 804 was mutated to phenylalanine (Y804F) using the

QuikChange Lightning Site-Directed Mutagenesis Kit (Agilent Technologies, 210518) with the following primers: 5'-ACTCAGCTAGT CCTAGGTTCATCTTACAATGCTCAG-3' and 5'-CTGAGCATTGTAAGATGAACCTAGGACTAGCTGAGT-3'. To create the TOP2A construct lacking the C-terminal domain (amino acids 1–1190), the MinSat-TOP2A plasmid was digested with Pfo I (Thermo Fisher Scientific, FD1754) to remove the C-terminal domain (amino acids 1191–1528), and the digested plasmid was used as a DNA template to synthesize the *MinSat-Top2a*^{ACTD} cRNA (see below). To create the TOP2A-targeting construct just with its C-terminal domain (amino acids 1208–1528, TOP2A^{CTD}), the following primers were used for the PCR amplification of TOP2A^{CTD}, 5'-ATGGACGAGCTGTACAAGTTGCCTCTCCTCGGG-3' and 5'-GTACCTTAAGCCTAGGTAGAAGAGTCGTCATCG-3'.

Oocyte microinjection

Germinal-vesicle-intact oocytes were microinjected with around 5 pl of cRNAs or antibodies in M2 containing 5 μM milrinone, using the TransferMan 4r and FemtoJet 4i (Eppendorf) micromanipulators. After the microinjection, oocytes were maintained at prophase I in M16 supplemented with 5 μM milrinone overnight to allow protein expression. cRNAs used for microinjections were *Ncapg2-Egfp* (*M. m. domesticus* or *M. spretus* NCAPG2 with eGFP at the C terminus) at 700 ng μl⁻¹, *Ncapg2-NES-Egfp* (*M. spretus* NCAPG2 with three tandem nuclear-export signals and eGFP at the C terminus) at 1,071 ng μl⁻¹, *Egfp-Ncapd3* (*M. m. domesticus* or *M. spretus* NCAPD3 with eGFP at the N terminus) at 700 ng μl⁻¹, *Ncaph2-Egfp* (*M. m. domesticus* or *M. spretus* NCAPH2 with eGFP at the C terminus) at 700 ng μl⁻¹, *Egfp-Top2a* (*M. m. domesticus* TOP2A fused to eGFP and LacI at the N terminus) at 430 ng μl⁻¹, *MinSat-Top2a* (TALE construct that recognizes *M. spretus* minor satellite repeats fused to mRuby2 and *M. m. domesticus* TOP2A at the C terminus) at 1,000 ng μl⁻¹, *MinSat-Top2a*^{ACTD} (TALE construct that recognizes *M. spretus* minor satellite repeats fused to mRuby2 and *M. m. domesticus* TOP2A (amino acids 1–1190) at the C terminus) at 1,016 ng μl⁻¹, *MinSat-Top2a*^{Y804F} (TALE construct that recognizes *M. spretus* minor satellite repeats fused to mRuby2 and *M. m. domesticus* catalytic-dead TOP2A^{Y804F} mutant at the C terminus) at 1,300 ng μl⁻¹, *MinSat-Top2a*^{CTD} (TALE construct that recognizes *M. spretus* minor satellite repeats fused to mRuby2 and *M. m. domesticus* TOP2A (amino acids 1208–1528) at the C terminus) at 613 ng μl⁻¹, *MajSat* (TALE construct that recognizes major satellite repeats fused to mClover and three tandem Halo tag at the C terminus) at 1,500 ng μl⁻¹ for live imaging and 3,000 ng μl⁻¹ for over-expression, *MinSat* (TALE construct that recognizes *M. spretus* minor satellite repeats fused to mRuby2 at the C terminus; Addgene, 47879) at 600 ng μl⁻¹ and *H2B-mCherry* (human histone H2B with mCherry at the C terminus) at 100 ng μl⁻¹. To TrimAway NCAPH2, *mCherry-Trim21* cRNA (*M. m. domesticus* TRIM21 fused to mCherry at the C terminus, Addgene, 105522) at 800 ng μl⁻¹ and normal rabbit IgG (Sigma-Aldrich, 12-370) or anti-NCAPH2 antibody (Invitrogen, pa5-66964) at 0.2 mg ml⁻¹ were co-microinjected⁵⁸. cRNAs were synthesized using the T7 mMessage mMachine Kit (Ambion, AM1340) and purified using the MEGAClear Kit (Thermo Fisher Scientific, AM1908).

Immunostaining of whole oocytes and chromosome spreads

Oocytes and eggs were fixed at prometaphase I (3 h from NEBD) or at metaphase I (7 h from NEBD) in freshly prepared 2% paraformaldehyde (Electron Microscopy Sciences, 15710) in 1× PBS (Quality Biological, 119-069-101CS) with 0.1% Triton X-100 (Millipore, TX1568-1) for 20 min at room temperature, permeabilized in 1× PBS with 0.1% Triton X-100 for 15 min at room temperature, placed in the blocking solution (0.3% BSA (Fisher Bioreagents, BP1600-100) and 0.01% Tween-20 (Thermo Fisher Scientific, J20605-AP) in 1× PBS) overnight at 4 °C, incubated 2 h with primary antibodies at room temperature, washed three times for 10 min with the blocking solution, incubated 1 h with secondary antibodies at room temperature, washed three times for 10 min in

the blocking solution and mounted onto microscope slides with the Antifade Mounting Medium with DAPI (Vector Laboratories, H-1200). To improve the immunostaining of NCAPD3 on metaphase chromosomes with the Bethyl antibody (A300-604A) in Fig. 5d and Extended Data Figs. 2a and 7a, zona pellucida was removed with acidic Tyrode's solution (Millipore, MR-004-D) 6 h after NEBD, incubated in M16 for 1 h, fixed with 2% paraformaldehyde in 1× PBS with 0.3% Triton X-100 for 30 min at 37 °C and incubated in the blocking/permeabilization solution (3% BSA in 1× PBS with 0.03% Triton X-100) overnight at 4 °C.

For chromosome spreads, zona pellucida was removed from oocytes, and the oocytes were fixed with 1% paraformaldehyde, 0.15% Triton X-100 and 3 mM DTT (Sigma-Aldrich, 43815) at metaphase I (7 h from NEBD).

For the cold stable microtubule assay (Extended Data Fig. 1e), oocytes were cultured for 6 h after NEBD and placed into ice-cold M2 for 3 min before fixation with freshly prepared 2% paraformaldehyde in 1× PBS with 0.1% Triton X-100 for 20 min at room temperature, permeabilized in 1× PBS with 0.1% Triton X-100 for 15 min at room temperature, and placed into the blocking solution (0.3% BSA and 0.01% Tween-20 in 1× PBS) overnight at 4 °C. Fixed oocytes were stained for α-tubulin, TOP2A and ACA (kinetochore). Centromeric TOP2A signals were used to distinguish *domesticus* and *spretus* centromeres.

The following primary antibodies were used: rabbit anti-mouse NCAPD3 (Figs. 2b, 3a and 4a,d and Extended Data Figs. 2b, 8a and 9b; 1:500, gift from T. Hirano), rabbit anti-mouse NCAPG (1:500, gift from T. Hirano) rabbit anti-human NCAPD3 (Fig. 5b,d and Extended Data Figs. 2a and 7a, 1:100, Bethyl, A300-604A), rabbit anti-human NCAPG2 (Fig. 3a; 1:100; Bioss, BS-7721R), rabbit anti-human NCAPG2 (Extended Data Fig. 6b,d; 1:100, Bethyl, A300-605A), rabbit anti-human NCAPH2 (1:100, Bethyl, A302-275A), goat anti-human SMC2 (1:100, Abcepta, AF2276a), rabbit anti-mouse SMC4 (1:100, Novus, NBP1-86635), CREST human autoantibody against centromere (1:100, Immunovision, HCT-0100), rabbit anti-topoisomerase II (1:100, Abcam, ab109524), goat anti-GFP antibody conjugated to Dylight488 (1:100, Rockland, 600-141-215). Secondary antibodies were Alexa Fluor 488-conjugated donkey anti-rabbit (1:500, Invitrogen, A21206) or donkey anti-goat (1:500, Invitrogen, A11057), Alexa Fluor 568-conjugated goat anti-rabbit (1:500, Invitrogen, A10042) or Alexa Fluor 647-conjugated goat anti-human (1:500, Invitrogen, A21445).

Bone marrow cell immunostaining

Bone marrow cells were collected from the femur by inserting a 26-G syringe needle into the cut end of the marrow cavity. Cells were flushed out into 3 ml of prewarmed DMEM high-glucose GlutaMAX medium (Gibco, 10566-016) supplemented with 10% FBS (Gibco, 10082147), 1 mM sodium pyruvate (Corning, 25-000-CL) and 1× antibiotic-antimycotic solution and incubated for 2 h at 37 °C in a humidified atmosphere of 5% CO₂ in air. The cells were pelleted twice at 500g for 5 min and resuspended in 1× PBS. Chromosome spreads and immunostaining were performed as described in the previous section.

Confocal microscopy

Fixed oocytes, eggs and bone marrow cells were imaged using a microscope (Eclipse Ti; Nikon) equipped with a ×100/1.40 NA oil-immersion objective lens, a CSU-W1 spinning-disk confocal scanner (Yokogawa), an ORCA Fusion Digital CMOS camera (Hamamatsu Photonics), and 405, 488, 561 and 640 nm laser lines controlled by the NIS-Elements imaging software (Nikon). Confocal images were acquired as z stacks at 0.3 μm intervals. For live imaging, oocytes were placed into 3 μl drops of M2 covered with paraffin oil in a glass-bottom tissue culture dish (fluoro-Dish, FD35-100) in a stage-top incubator (Tokai Hit) to maintain 37 °C. Time-lapse images were collected with a microscope (Eclipse Ti2-E; Nikon) equipped with a ×20/0.75 NA objective (Fig. 1b and Extended Data Fig. 1a) and a ×60/1.40 NA oil-immersion objective (Fig. 1d), a CSU-W1 spinning disk confocal scanner (Yokogawa), an ORCA Fusion

Digital CMOS camera (Hamamatsu Photonics), and 405, 488, 561 and 640 nm laser lines controlled by the NIS-Elements imaging software (Nikon). Confocal images were collected as z stacks at 1 μm intervals to visualize all of the chromosomes. Images are displayed as maximum intensity z projections.

Image analysis

ImageJ (NIH) was used to analyse all of the images. In general, optical slices containing chromosomes were added to produce a sum intensity z projection for pixel intensity quantifications. To quantify centromeric signal intensities (NCAPD3 and TOP2A), ellipses were drawn to encompass minor satellites (Fig. 4d (*spretus* centromeres)) or major satellites (Fig. 4b,d (*domesticus* centromeres) and 5c and Extended Data Figs. 2b and 10a,b) of each chromosome based on MinSat TALE signals and the DAPI staining, and the signal intensity was integrated over each ellipse after subtracting background signals, obtained near the centromere. To specifically quantify kinetochore NCAPD3 signal intensities, ellipses were drawn around each kinetochore based on the ACA staining, and the signal intensity was integrated over each ellipse after subtracting background signals, obtained near the kinetochore. As NCAPD3 levels were variable among *domesticus* × *spretus* hybrid oocytes, with some oocytes having chromosomal NCAPD3 signals barely above the cytoplasmic background (Extended Data Fig. 2a,c), we focused our analyses on hybrid oocytes with detectable NCAPD3 signals when analysing condensin II localization patterns within the chromosome (Fig. 4a,d). To quantify TOP2A signal intensities on the chromosome axis, ellipses were drawn on the chromosome axis avoiding the centromere region based on the DAPI and centromeric TOP2A staining, and the signal intensity was integrated over each ellipse after subtracting the background signals, obtained near the chromosome. To quantify signal intensities on the entire chromosome (NCAPD3, NCAPG, NCAPG2-eGFP and NCAPG2-NES-eGFP), masking images were created using DAPI staining images to specifically measure signal intensities on the chromosome. The signal intensity was integrated over each slice after subtracting background signals, obtained near the chromosomes. To quantify signal intensities in the nucleus (NCAPD3, NCAPG2, NCAPH2, SMC2 and SMC4), ellipses were drawn around the entire nucleus (including the nucleolus, which has lower signal intensities), and the signal intensity was integrated over each ellipse after subtracting the background signals, obtained near the nucleus. For the nuclear levels of NCAPG2-eGFP and NCAPG2-NES-eGFP (Extended Data Fig. 7b), we measured the nuclear/cytoplasmic ratio because the typical cytoplasm background subtraction would lead to negative values for signal intensities of NCAPG2-NES-eGFP, which has higher signals in the cytoplasm compared with in the nucleus. For the *in situ* chromosome counting assay, the number of chromosomes was counted in metaphase II eggs using the DAPI and ACA (kinetochore) signals³⁹.

Western blot

Each oocyte sample contained 100 oocyte cells, and each thymus sample contained 5 mg of the thymus tissue. Thymus tissues were homogenized using the RIPA buffer (150 mM NaCl (Millipore, 116224), 0.5% sodium deoxycholate (Biochemica, A1531) and 50 mM Tris, pH 8.0 (KD Medical, RGF-3360) and 1% Triton X-100) supplemented with the protease inhibitor cocktail (MedChem Express, HY-K0010). Oocyte samples and thymus cell extracts were mixed with Laemmli buffer (Bio-Rad, 1610737) containing β-mercaptoethanol (Sigma-Aldrich, M6250) and denatured at 95 °C for 5 min. The samples were separated on 10% Mini-Protean TGX Precast Protein Gels (Bio-Rad, 4561036) or on 10% Mini-Protean TGX Stain-Free Protein Gels (Bio-Rad, 4568036) to visualize the total proteins using the GelDoc Go Gel Imaging System (Bio-Rad, 12009077) before the transfer. Proteins were transferred to the PVDF membrane (Bio-Rad, 1704156) using the Trans-Blot Turbo Transfer System (Bio-Rad), and blocked for 1 h at room temperature with 2% ECL Prime Blocking agent (Cytiva, RPN418V). The membrane

Article

was then incubated overnight at 4 °C with the rabbit anti-human NCAPG2 (1:300, Bioss, BS-7721R), then washed three times for 15 min each with the TBST buffer (20 mM Tris, pH 7.6, 150 mM NaCl and 0.1% Tween-20) and incubated for 1 h with the rabbit peroxidase-conjugated secondary antibody (Bethyl, A120-201P), which was detected using the ECL detection reagents (Bio-Rad, 1705061) and Amersham Imager 600 (GE Healthcare).

Statistics and reproducibility

Data points were pooled from two to five independent experiments, and the exact number of independent experiments for each experimental group is listed in Supplementary Table 1. Data analysis was performed using Microsoft Excel and GraphPad Prism 10. Scattered plots and line graphs were created using GraphPad Prism 10. Two-sided unpaired *t*-tests were used for statistical analysis unless specified in the figure legend, and the actual *P* values are shown in each figure legend. The sample size was chosen on the basis of current practices in the field. Randomization is built into the experiments because each animal was chosen from a different litter and mating pair and no data were excluded and all cells were imaged at random. Investigators were not blinded for data collection and quantification as the phenotype automatically reports on the genotype consistently.

Reporting summary

Further information on research design is available in the Nature Portfolio Reporting Summary linked to this article.

Data availability

The datasets analysed during the current study are available at Figshare (<https://doi.org/10.25444/nhlbi.23671194>). Source data are provided with this paper.

55. Iwata-Otsubo, A. et al. Expanded satellite repeats amplify a discrete CENP-A nucleosome assembly site on chromosomes that drive in female meiosis. *Curr. Biol.* **27**, 2365–2373 (2017).
56. Stein, P. & Schindler, K. Mouse oocyte microinjection, maturation and ploidy assessment. *J. Vis. Exp.* <https://doi.org/10.3791/2851> (2011).
57. Igashiki, H., Knott, J. G., Schultz, R. M. & Williams, C. J. Alterations of PLC β 1 in mouse eggs change calcium oscillatory behavior following fertilization. *Dev. Biol.* **312**, 321–330 (2007).
58. Ostromyshenskii, D. I., Kuznetsova, I. S., Golinishchev, F. N., Malikov, V. G. & Podgornaia, O. I. Satellite DNA as a phylogenetic marker: case study of three genera of the Murinae subfamily. *Tsitolgiia* **53**, 564–571 (2011).
59. Tada, K., Susumu, H., Sakuno, T. & Watanabe, Y. Condensin association with histone H2A shapes mitotic chromosomes. *Nature* **474**, 477–483 (2011).
60. Samoshkin, A. et al. Human condensin function is essential for centromeric chromatin assembly and proper sister kinetochore orientation. *PLoS ONE* **4**, e6831 (2009).
61. Clift, D. et al. A method for the acute and rapid degradation of endogenous proteins. *Cell* **171**, 1692–1706 (2017).
62. Shintomi, K. & Hirano, T. Guiding functions of the C-terminal domain of topoisomerase II α advance mitotic chromosome assembly. *Nat. Commun.* **12**, 2917 (2021).

Acknowledgements We thank A. E. Kelly, N. M. Rusan and N. Phadnis for comments on the manuscript; M. A. Lampson, B. E. Black and the members of the Akera laboratory for discussions; T. Hirano for the NCAPD3 and NCAPG antibodies; and M. E. Torres-Padilla and Y. Miyanari for the TALE constructs. Schematics in the figures were created using BioRender. This work was funded by Division of Intramural Research at the National Institutes of Health/National Heart, Lung and Blood Institute (1ZIAHL006249 to T.A.).

Author contributions Conceptualization: T.A. Methodology: W.E.Y. and T.A. Investigation: W.E.Y. and T.A. Funding acquisition: T.A. Supervision: T.A. Writing—original draft: W.E.Y. Writing—review and editing: W.E.Y. and T.A.

Competing interests The authors declare no competing interests.

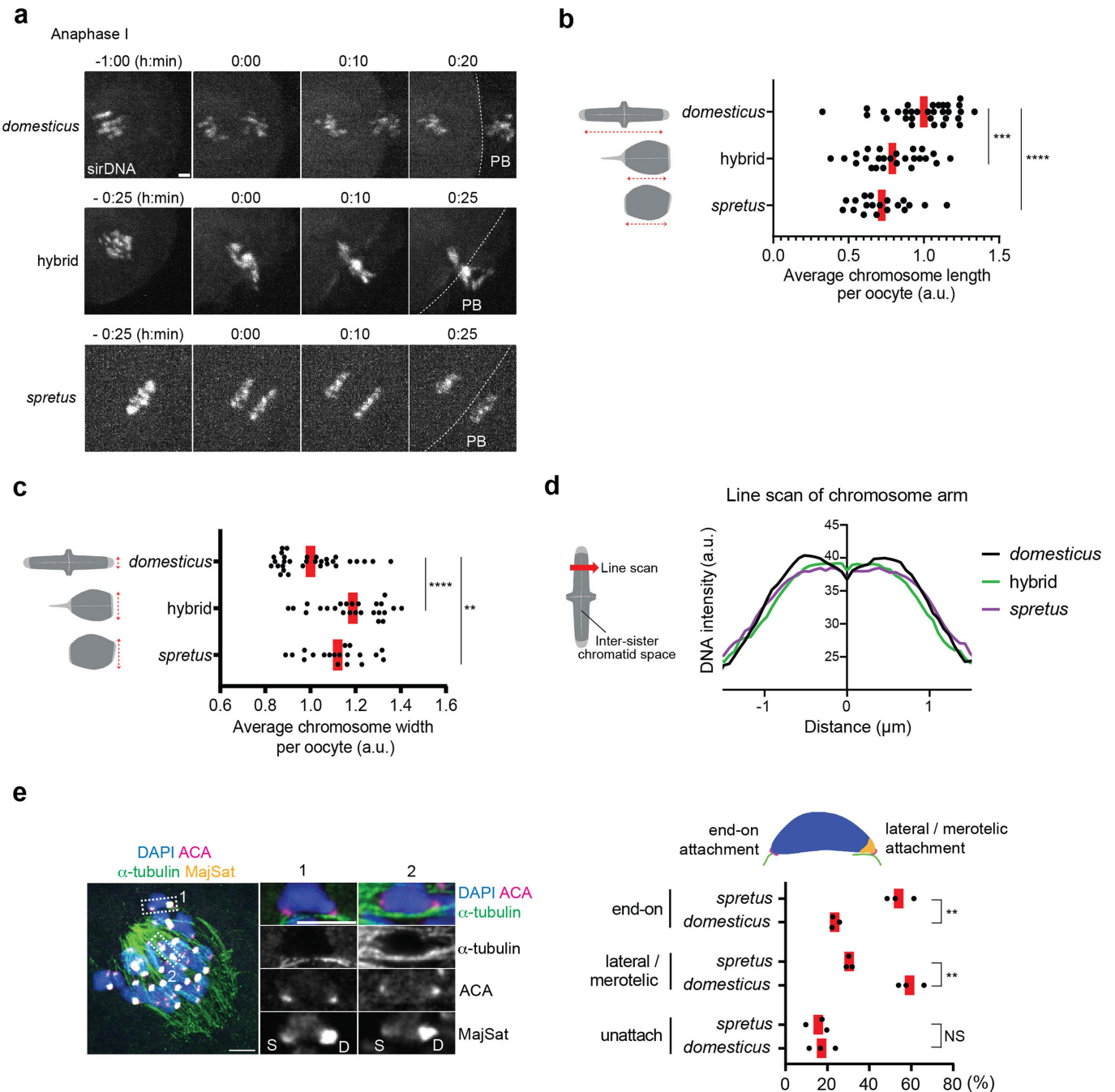
Additional information

Supplementary information The online version contains supplementary material available at <https://doi.org/10.1038/s41586-023-06700-6>.

Correspondence and requests for materials should be addressed to Takashi Akera.

Peer review information *Nature* thanks the anonymous reviewers for their contribution to the peer review of this work. Peer reviewer reports are available.

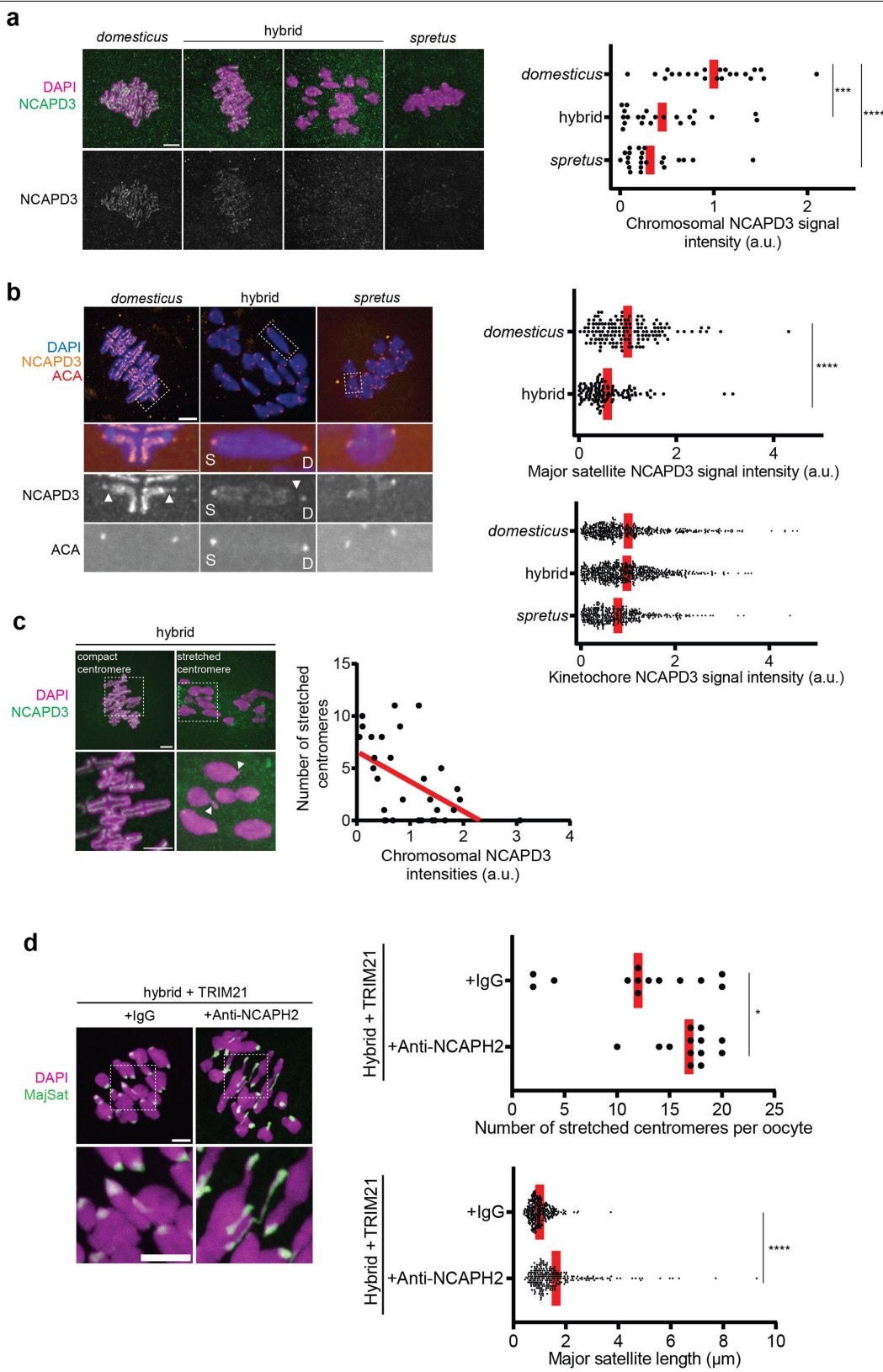
Reprints and permissions information is available at <http://www.nature.com/reprints>.



Extended Data Fig. 1 | Morphologically distinct chromosomes in hybrid and spretus oocytes. **a**, *domesticus*, hybrid and *spretus* oocytes were imaged live in anaphase I in the presence of sirDNA to visualize chromosomes. PB, polar body; dashed lines, oocyte cortex. See Fig. 1b for the quantification of the lagging chromosome rate. **b,c**, The chromosome length (**b**) and width (**c**) were quantified. Each dot in the graph represents a single oocyte (**b**, $n = 26, 21$ and 21 oocytes for *domesticus*, hybrid and *spretus*, respectively; **c**, $n = 31, 25$ and 19 oocytes for *domesticus*, hybrid and *spretus*, respectively); unpaired t-test (two-sided) was used for statistical analysis; $**P = 0.0042$, $***P < 0.0007$, $****P < 0.0001$. **d**, The graph shows line scans of the DNA intensity across the chromosome arm region to quantify the individualization of sister chromatids. *domesticus* chromosomes tend to be more individualized, indicated by the dip in the DNA intensity in the middle of the line scan (i.e., inter-sister chromatid space), compared to hybrid and *spretus* chromosomes. The line scans are averaged over $n = 188, 121$ and 154 chromosomes for *domesticus*, hybrid and *spretus*, respectively. **e**, hybrid oocytes were analysed for cold-stable

microtubules at metaphase I. Enlarged images are optical slices showing individual bivalents with the *spretus* centromere correctly attached to the spindle (i.e., end-on attachment), whereas the *domesticus* centromere has lateral/merotelic attachment. We speculate that major satellite stretching would reduce the abundance of the error-correction machinery (i.e., Aurora B kinase and MCAK) localized at the pericentromere, leaving mis-attachments at *domesticus* centromeres uncorrected. Consistent with this idea, knocking down condensin in mitosis reduces Aurora B kinase at pericentromeres⁶⁰. Furthermore, we previously reported that *domesticus* centromeres have less MCAK compared to *spretus* centromeres⁵¹. The uncorrected mis-attachments would eventually cause lagging chromosomes in anaphase as observed in **a**. The graph shows the percentage of centromeres in each attachment category; each dot represents an independent experiment ($n = 63, 62$ and 66 bivalents analysed in each experiment); unpaired t-test (two-sided) was used for statistical analysis; NS = 0.7457 , $**P = 0.0014$ (lateral/merotelic), $**P = 0.0015$ (end-on); red line, mean; scale bar: $5 \mu\text{m}$.

Article

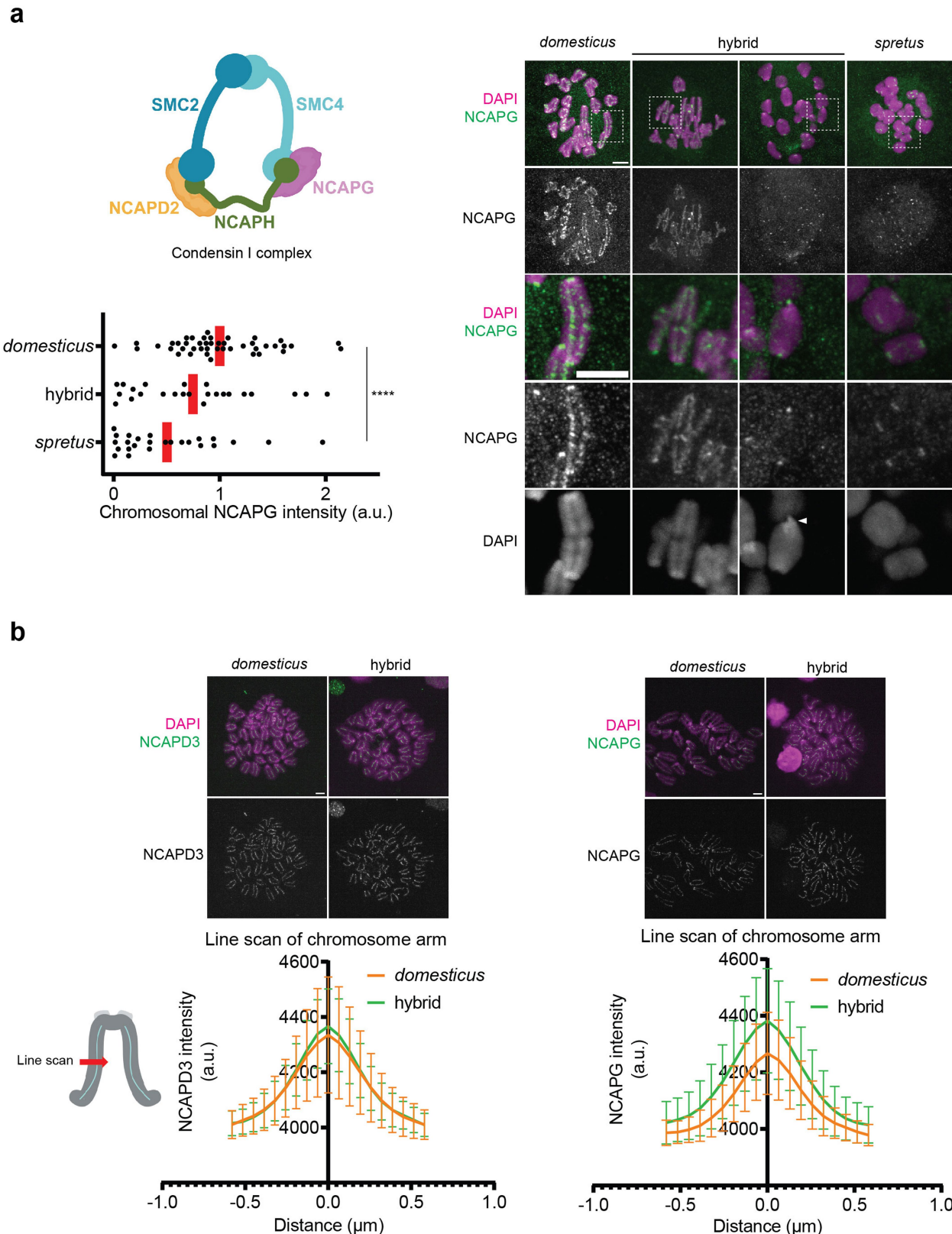


Extended Data Fig. 2 | See next page for caption.

Extended Data Fig. 2 | Reduced condensin II abundance leads to centromere stretching in hybrid oocytes. **a**, *domesticus*, hybrid and *spretus* oocytes were fixed at metaphase I and stained for NCAPD3, using a different antibody (Bethyl, A300-604A) from Fig. 2b where the NCAPD3 antibody from the Hirano lab was used. NCAPD3 intensities on the chromosome were quantified, showing a similar trend with Fig. 2b ($n = 22, 22$ and 23 oocytes for *domesticus*, hybrid and *spretus*, respectively); each dot in the graph represents a single oocyte; unpaired t-test (two-sided) was used for statistical analysis; *** $P = 0.0002$, **** $P < 0.0001$; red line, mean. **b**, *domesticus*, hybrid and *spretus* oocytes were fixed at metaphase I and stained for NCAPD3 and ACA (kinetochores) (dataset from Fig. 2b). NCAPD3 intensities at major satellites (white arrowheads in the images, top graph, $n = 16$ and 15 oocytes for *domesticus* and hybrid, respectively) and kinetochores (bottom graph, $n = 32, 26$ and 21 oocytes for *domesticus*, hybrid and *spretus*, respectively) were quantified; each dot in the graph represents a single centromere; unpaired t-test (two-sided) was used for statistical analysis; **** $P < 0.0001$; red line, mean. NCAPD3 levels at major satellites were reduced in hybrid oocytes compared to *domesticus* oocytes, consistent with the idea that reduced condensin II at major satellites drives centromere stretching in hybrid oocytes. Kinetochore NCAPD3 intensities were similar among *domesticus*, hybrid and *spretus* oocytes, indicating that the kinetochore condensin II pool is regulated differently from the rest of the

chromosome, similar to fission yeast condensin⁵⁹. This analysis suggests that the *spretus* genetic background reduces the condensin II abundance on the chromosome axis and centromeric satellites but not as much at the kinetochore. **c**, Hybrid oocytes were fixed at metaphase I and stained for NCAPD3 (dataset from Fig. 2b plus one additional independent experiment). Chromosomal NCAPD3 intensities relative to the number of stretched centromeres per oocyte were plotted in the graph ($n = 31$ oocytes); white arrowheads, stretched centromeres; red line, a simple linear regression between chromosomal NCAPD3 intensities and the number of stretched centromeres ($R^2 = 0.2595$, $P < 0.0034$). **d**, To partially deplete NCAPH2 by the TrimAway method⁶¹, hybrid oocytes expressing mCherry-Trim21 with the control IgG or the anti-NCAPH2 antibody microinjection were fixed at prometaphase I and stained for TOP2A (a major satellite marker, Extended Data Fig. 8b). The number of stretched centromeres per oocyte (top graph; $n = 13$ and 13 cells for + IgG and + anti-NCAPH2 antibody, respectively) and the major satellite length was quantified (bottom graph; $n = 277$ and 259 centromeres for + IgG and + anti-NCAPH2 antibody, respectively); unpaired t-test (two-sided) was used for statistical analysis; * $P = 0.015$, **** $P < 0.0001$. Images are maximum intensity z projections to show all chromosomes or optical slices magnified to show individual chromosomes; red line, mean; scale bars: $5 \mu\text{m}$.

Article

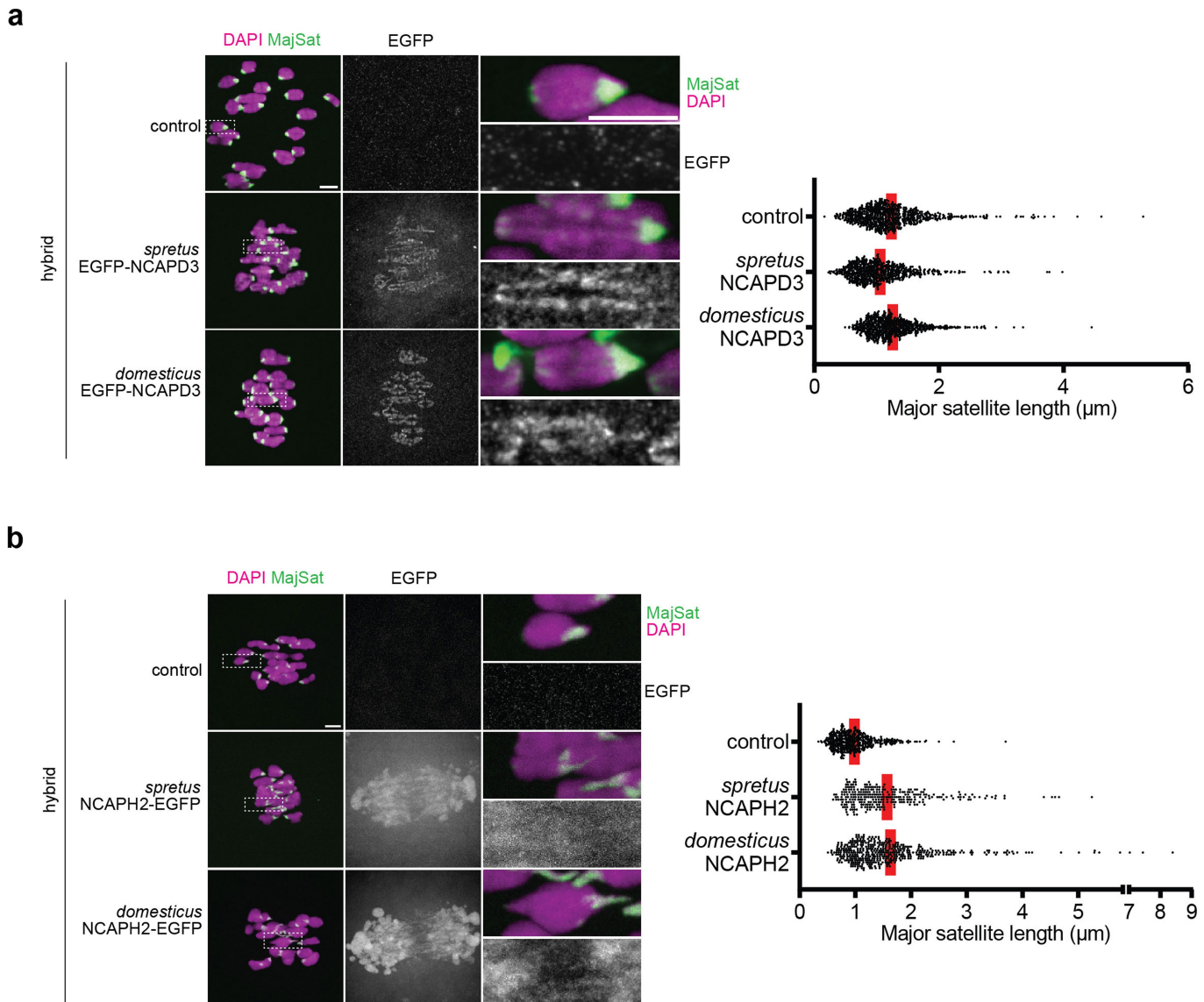


Extended Data Fig. 3 | See next page for caption.

Extended Data Fig. 3 | Localization of condensin I and II in hybrid oocytes and somatic cells. **a**, Schematic of the condensin I complex. *domesticus*, hybrid and *spretus* oocytes were fixed at metaphase I and stained for NCAPG (condensin I). NCAPG intensities on the chromosome were quantified, showing a similar trend with condensin II ($n = 44, 24$ and 25 oocytes for *domesticus*, hybrid and *spretus*, respectively; each dot in the graph represents a single oocyte; unpaired t-test (two-sided) was used for statistical analysis; *** $P < 0.0001$; red line, mean. Condensin I levels were variable among hybrid oocytes similar to condensin II (Extended Data Fig. 2c) and more often than not were lower compared to *domesticus* oocytes ($P = 0.0539$). **b**, Chromosomes were spread

using bone marrow cells isolated from *domesticus* and the hybrid and stained for NCAPD3 and NCAPG. The graph shows line scans of the NCAPD3 and NCAPG intensity across the chromosome arm region to quantify the chromosome axis enrichment of condensin II and I, respectively. Condensin II levels were similar between *domesticus* and the hybrid, whereas condensin I levels were slightly higher in the hybrid. The NCAPD3 line scans were averaged over $n = 100$ and 100 chromosomes for *domesticus* and hybrid, respectively, and the NCAPG line scans were averaged over $n = 100$ and 100 chromosomes for *domesticus* and hybrid, respectively; error bars, standard deviation; scale bars: $5 \mu\text{m}$. The schematic in **a** and **b** was created using BioRender.

Article



Extended Data Fig. 4 | Overexpressing NCAPD3 or NCAPH2 did not rescue centromere stretching. Hybrid oocytes expressing eGFP-NCAPD3 (a) or NCAPH2-eGFP (b) derived from *domesticus* or *spretus* were fixed at prometaphase I and stained for TOP2A (a major satellite marker, see Extended Data Fig. 8b) and eGFP. The length of major satellites was quantified; each dot in the graph represents a single centromere (a, n = 752, 683 and 743 centromeres for control, + *spretus* eGFP-NCAPD3 and + *domesticus* eGFP-NCAPD3, respectively; b, n = 464, 294 and 451 centromeres for control, + *spretus*

NCAPH2-eGFP and + *domesticus* NCAPH2-eGFP, respectively). NCAPH2-eGFP was not able to localize on the chromosome probably because of the competition with endogenous NCAPH2²⁹. The enhanced centromere stretching upon overexpressing NCAPH2-eGFP implies that NCAPH2-eGFP sequesters other condensin II subunits in the cytoplasm, reducing the functional condensin II pool. Images are maximum intensity z projections to show all chromosomes or optical slices to show individual chromosomes; red line, mean; scale bars: 5 μm .

a NCAPG2

human	MEKRETFVQAVSKELVGEFLQFVLQDFSLNLELDELSRKQKEELWLQRQLNLLTDLVILSPVDQWVQEAGEDNNMETHEGSKMRKSIEIIYIAVTVIASVSIENESYEALL	120
musculus	MEKRETFVQAVSKELVGEFLQFVLQDFSLNLELDELSRKQKEELWLQRQLNLLTDLVILSPVDQWVQEAGEDNNMETHEGSKMRKSIEIIYIAVTVIASVSIENESYEALL	120
spretus	MEKRETFVQAVSKELVGEFLQFVLQDFSLNLELDELSRKQKEELWLQRQLNLLTDLVILSPVDQWVQEAGEDNNMETHEGSKMRKSIEIIYIAVTVIASVSIENESYEALL	120
*****	*****	*****
human	ECVI1LNGLYALPALSERKLQSS1QDLCVTTWEKGPAKEDTGKTAFLVMRLRBSLETKTGADCVLRWLIHQALYCFDYLDEESGEIKDMLLECFININVINYIKKEGRRFLSCLFNWNINF	240
musculus	ECAVILNGLYALPALSERKLQSS1QDLCVTTWEKGPAKEDTGKTAFLVMRLRBSLETKTGADCVLRWLIHQALYCFDYLDEESGEIKDMLLECFININVINYIKKEGRRFLSCLFNWNINF	240
spretus	ECAVILNGLYALPALSERKLQSS1QDLCVTTWEKGPAKEDTGKTAFLVMRLRBSLETKTGADCVLRWLIHQALYCFDYLDEESGEIKDMLLECFININVINYIKKEGRRFLSCLFNWNINF	240
*****	*****	*****
human	KMIHGTIKNQLQGLQKSLMVYIAEIJYFRAWKKASKGKLEATIENDC1QDFMFHGHLPLRRSPVHSVKREVLSYFHQQKVKVRQGEVEMLYRLYKPLILWRGLKARNSEVRNSAALLFVEAFPI	360
musculus	KMIHETIKNQLAGLQKSLMVHIAEIJYFRAWKKASKGKLEATIENDC1QDFMFHGHLPLRRSPVHSVKREVLSYFHQQKVKVRQGEVEMLYRLYKPLILWRGLKARNSEVRNSAALLFVEAFPI	359
spretus	KMIHETIKNQLAGLQKSLMVHIAEIJYFRAWKKASKGKLEATIENDC1QDFMFHGHLPLRRSPVHSVKREVLSYFHQQKVKVRQGEVEMLYRLYKPLILWRGLKARNSEVRNSAALLFVEAFPI	359
*****	*****	*****
human	RDPNLHAIEMDSEI1QKQFEELYSLLLEDPPMVRTGILGVCKITSKYWEMMPPTILLIDLLKVTLGELAFDTSSADVRCSVFKCLPMLIDTRISHPLLEQDLPALRYSLDHNSEKRVAFV	480
musculus	RDPNFIATEMDNEI1QKQFEELYNLIEDPYPRVSTGILGVCKLISSSKWMPEPPNLLIDVFLKVTLGELAFDISSADVRCSVFKCLPILIDLNKLSPHLLEQDLPTRLYSLHDNSEKRVAFV	479
spretus	RDPNFATEMDSEI1QKQFEELYNLIEDPYPRVSTGILGVCKLISSSKWMPEPPNLLIDVFLKVTLGELAFDISSADVRCSVFKCLPILIDLNKLSPHLLEQDLPTRLYSLHDNSEKRVAFV	479
*****	*****	*****
human	DLLLKIKAVERAKRAFKWICPMEDILVRLEMDSRPSVRSLLSFLINSPVNPQEEWCERCVTLIQMNRAARRFYQYAHETNSTNIAKLHIVIRHCLNACIQRTLREGS YEAH --KECE	600
musculus	DLLLKIKAVERAKRAFKWICPMEDILVRLEMDSRPSVRSLLSFLINSPVNPQEEWCERCVTLIQMNRAARRFYQYAHETNSTNIAKLHIVIRHCLNACIQRTLREGS YEAH --KECE	596
spretus	DLLLKIKAVERAKRAFKWICPMEDILVRLEMDSRPSVRSLLSFLINSPVNPQEEWCERCVTLIQMNRAARRFYQYAHETNSTNIAKLHIVIRHCLNACIQRTLREGS YEAH --KECE	596
*****	*****	*****
human	KENVTVLTKLTSVNDVACMAGLLEIIVLWKS1DRSMMENKEAKLYTINKFASVLPPEYLKVFKDRCK1PLFMLMSFMPASAVPPFCGV1TLRSREEGAVDKSYCTLLDCLSQGWQVG	720
musculus	KENASVLDKLTSLVNTDASMAGLLEIIVLWKN1IHSRLENNKEAKIYTINKFAAVLPPEYLKVFKDRCK1PLFMLMSF F PASAVPVFCGV1SVLRNQ-EVTGRSYCTLLDCLSQGWQVG	715
spretus	KENASVLDKLTSLVNTDASMAGLLEIIVLWKN1IHSRLENNKEAKIYTINKFAAVLPPEYLKVFKDRCK1PLFMLMSF F PASAVPVFCGV1SVLRNQ-EVTGRSYCTLLDCLSQGWQVG	715
*****	*****	*****
human	HILELVNDNLWLPTEHAQAKNSNTASKGRVQIHDTRPVKPELALVYIEYLLTHPKNRECLLSAPRKKLNLHLLKALETSKADLESLLQTPGKGKPRGFSEAAAPRAFGLHCRLS1HLOHKFCSEG	840
musculus	HVLELVNDWLWLPTEHAQAKNSNTASKGRVQIHDTRPVKPELALVYIEYLLTHPKNRECLLSAPRKKLNLHLLKALETSKADLESLLQTPGKGKPRGFSEAAAPRAFGLHCRLS1HLOHKFCSEG	835
spretus	HVLELVNDWLWLPTEHAQAKNSNTASKGRVQIHDTRPVKPELALVYIEYLLTHPKNRECLLSAPRKKLNLHLLKALETSKADLESLLQTPGKGKPRGFSEAAAPRAFGLHCRLS1HLOHKFCSEG	835
*****	*****	*****
human	KVYSLSMSLEDTGFWLESKLSFIQDQEEYDYLKLHRYIYQQI1QTYLTVCKDVMVGLGDHQFQMOLLQSRSLGIMQTVKGFYVSLLDILKEITGSSL1QKTDSEEVAMLLDTVQVFQK	960
musculus	KIHL5L1DDDTGSWLENKVLPLLEDQEEYDYLKLHRYIYQQI1QTYLTVCKDVMVGLG G PKFQMOLLQSRSGIMKTVKGFYVSLLDILKEITGSSL1QKTDSEEVAMLLDTVQVFQK	955
spretus	KIHL5L1DDDTGSWLENKVLPLLEDQEEYDYLKLHRYIYQQI1QTYLTVCKDVMVGLG G PKFQMOLLQSRSGIMKTVKGFYVSLLDILKEITGSSL1QKTDSEEVAMLLDTVQVFQK	955
*****	*****	*****
human	MLECIARSFRQKPEEGRLRLYSSVQRPLHEFITAVQSRHLDTPVHRGVLSLTLIAGPVVEISHQLRKVSDEELTPPEHLSLDPFFSRLCLIGIIKSSNVRSFLDELKACVASNDIEGIVC	1080
musculus	MLECIACIFCRQKPEEGRLPLFHSV1PLTHEFT1TQSQRHWDATAVHLTLIAAFVEISHQLRKVSDEELTPCQLHDPFFSRLCVLGVMKSDVURSF Y DELKACVTSGDEVGIVC	1075
spretus	MLECIACIFCRQKPEEGRLPLFHSV1PLTHEFT1TQSQRHWDATAVHLTLIAAFVEISHQLRKVSDEELTPCQLHDPFFSRLCVLGVMKSDVURSF Y DELKACVTSGDEVGIVC	1075
*****	*****	*****
human	LTAAVH1LIVNAGKHKS NVEVAJATVHNK1KTFME1TLEEDS1ERIE1D1 LCPCGWA1TPGLLDST1YFSASVPI C	1156
musculus	LTAVAL1LIVNAGKHKS NVEVAJATVHNK1KTFME1TLEEDS1ERIE1D1 LCPCGWA1TPGLLDST1YFSASVPI C	1138
spretus	LTAVAL1LIVNAGKHKS NVEVAJATVHNK1KTFME1TLEEDS1ERIE1D1 LCPCGWA1TPGLLDST1YFSASVPI C	1138
*****	*****	*****

b NCAPD3

human	1450	SQGNNDILCLSLSPDKPPFPQQPNWKS PARNSHGSTRSRRSLRKAPLTKN	1498
musculus	1458	EQGSDILCLSLSDKRPFQSPQWNWKS PARSHGSTRSRRSLRKAPLTKN	1506
spretus	1455	EQGSDILCLSLSDKRPFQSPQWNWKS PARSHGSTRSRRSLRKAPLTKN	1503
spicilegus	1459	EQGSDILCLSLSDKRPFQSPQWNWKS PARSHGSTRSRRSLRKAPLTKN	1507

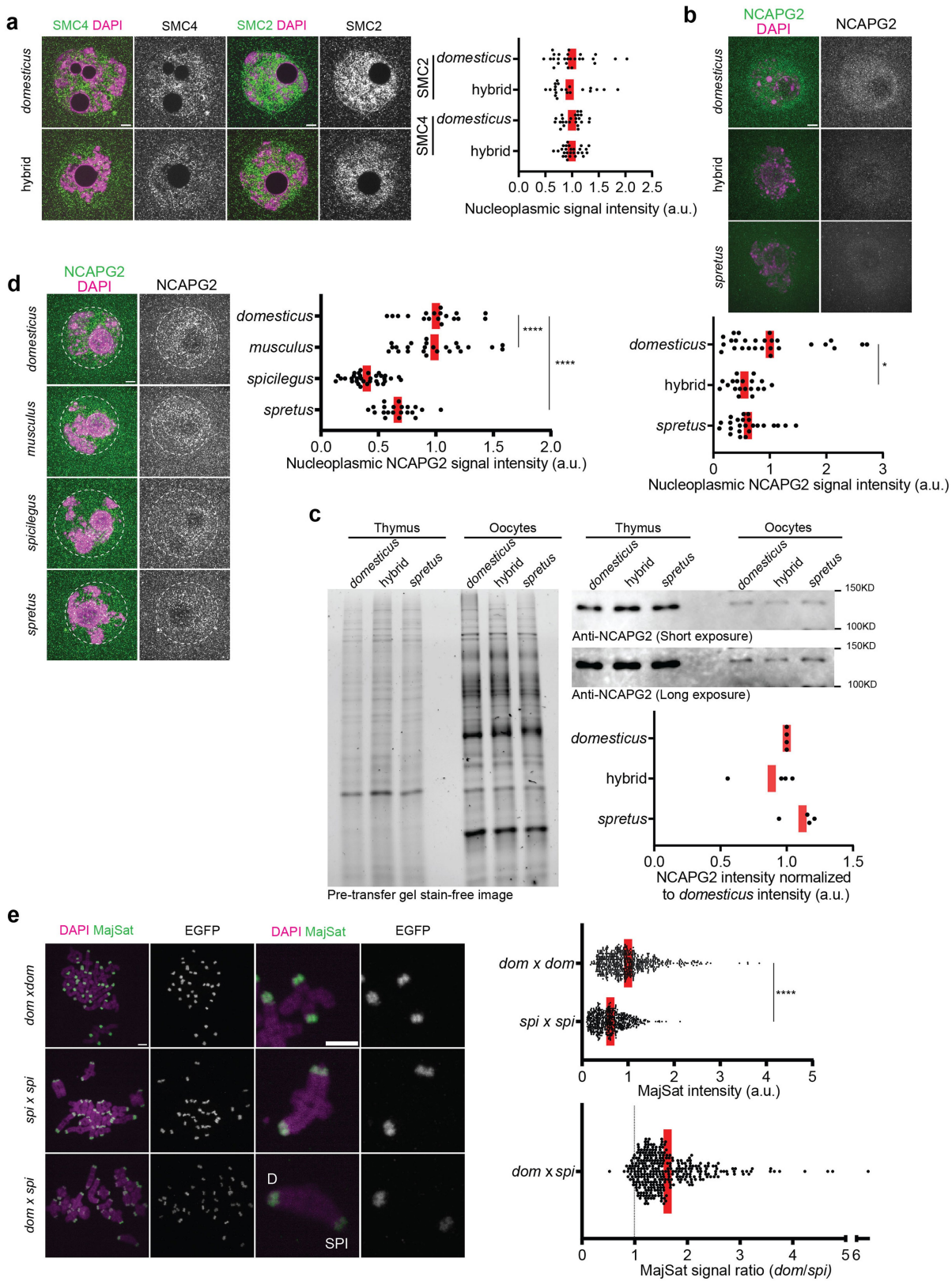
C NCAPG2

human	1100	KVREVAATVHRKLKTFMEITLEEDS I ERYEDL--LCCPGWALTPGLLDSIYPSASVPIG	1156
musculus	1097	KVKVEAVVYVYRKLKTFMEITLEEDSLERLYFESSMRTLGEFLNP--	1138
spretus	1097	KVKEVAATVYVYRKLKTFMEITLEEDSLERLYFESSMRTLGEFLNP--	1138
spicilegus	1097	KVKEVAASAVYVYRKLKTFMEITLEEDSLERLYFESSMRTLGEFLNP--	1138

Extended Data Fig. 5 | NCAPG2 amino acid sequences are mostly conserved between *domesticus* and *spretus*. **a.** The entire amino acid sequences of NCAPG2 from *H. sapiens*, *M. musculus domesticus* (*musculus*), and *M. spretus* were aligned. Residues diverged between *domesticus* and *spretus* were highlighted in yellow. Although there are several residues diverged between *domesticus* and *spretus* NCAPG2, these differences are probably not part of the hybrid incompatibility, because both of them showed similar localization pattern and efficiently rescued centromere stretching when overexpressed in hybrid oocytes (Fig. 2c and Extended Data Fig. 7b). NCAPG2 antibodies used in this study (Bioss bs-7721R and Bethyl A300-605A) were raised against human NCAPG2 fragments. Antigen sequences used for the antibody productions

were highlighted in light green for the Bioss antibody and light blue for the Bethyl antibody. **b,c**, Part of the amino acid sequences of human NCAPD3 (**b**) and NCAPG2 (**c**) that were used as the antigens (highlighted in grey) to produce the Bethyl A300-604A and A300-605A antibodies were aligned with NCAPD3 and NCAPG2 sequences from *M. musculus domesticus*, *M. spretus* and *M. spicilegus*. A single residue diverged among mouse species were highlighted in yellow. Since the sequences are basically conserved across the mouse species for the region corresponding to the antigen sequences (**a-c**), it is unlikely that the distinct NCAPG2 and NCAPD3 staining patterns among these mouse species are due to the differential efficiency in antibody recognition (Figs. 2b, 3a, 5b, d and Extended Data Fig. 2a, 6b, d).

Article



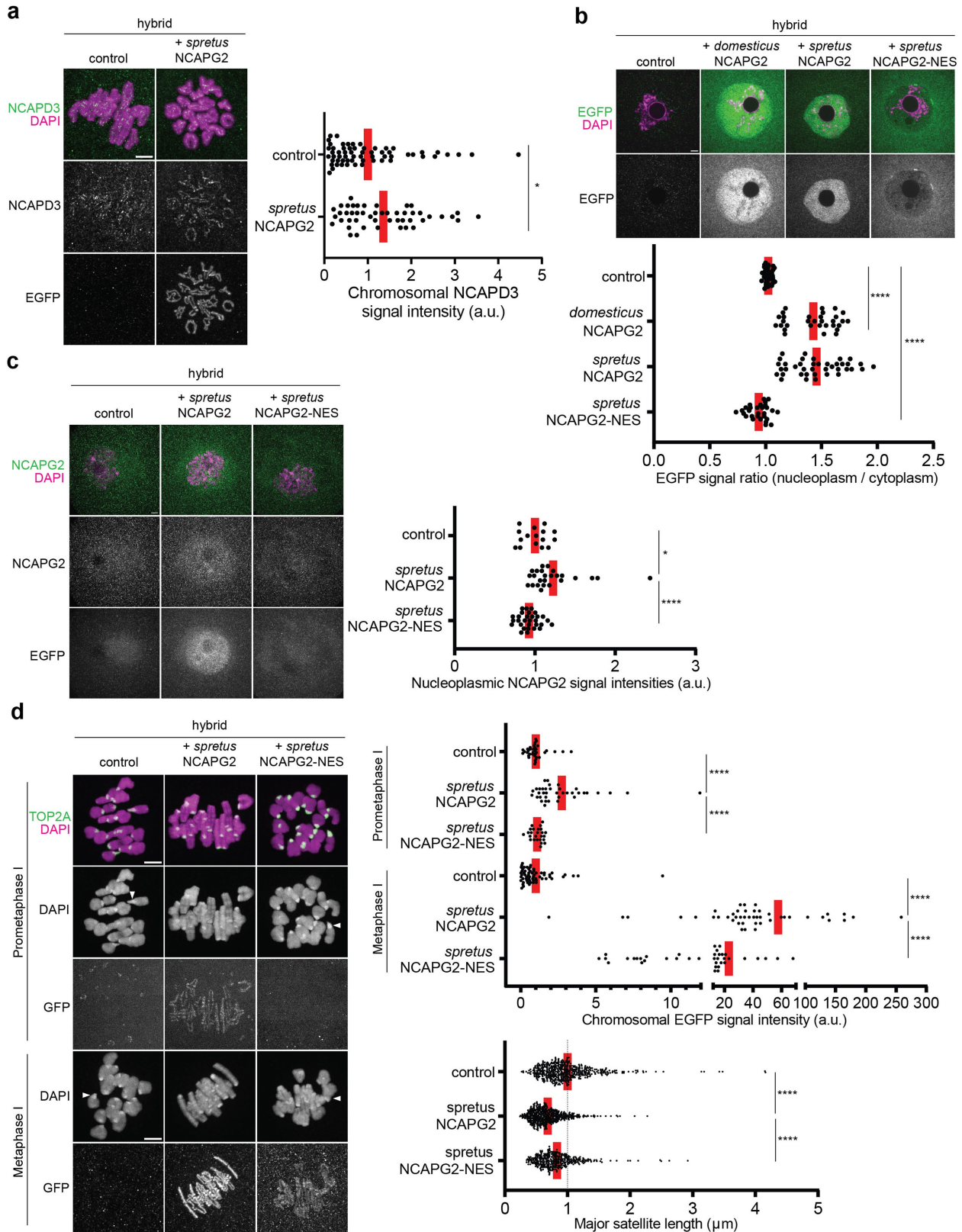
Extended Data Fig. 6 | See next page for caption.

Extended Data Fig. 6 | Nuclear enrichment of condensin II subunits in late prophase I. **a**, *domesticus* and hybrid oocytes were fixed at prophase I and stained for SMC2 and SMC4. The graph shows the quantification of SMC2 and SMC4 intensities in the nucleus; each dot in the graph represents a single oocyte (SMC2: n = 26 and 21 oocytes for *domesticus* and hybrid, respectively; SMC4: n = 24 and 27 oocytes for *domesticus* and hybrid, respectively).

b, *domesticus*, hybrid and *spretus* oocytes were fixed at prophase I and stained for NCAPG2 (Bethyl A300-605A). The graph shows the quantification of NCAPG2 intensities in the nucleus, which shows a similar trend with Fig. 3a where a different NCAPG2 antibody (Bioss bs-7721R) was used; each dot in the graph represents a single oocyte (n = 27, 19 and 24 oocytes for *domesticus*, hybrid and *spretus*, respectively); unpaired t-test (two-sided) was used for statistical analysis; *P = 0.015. **c**, Western blot of NCAPG2 using thymus tissues and oocyte samples. As a loading control, stain-free gel image was shown to indicate the total protein amount loaded to each lane. Oocyte collection and western blot were repeated four times to quantify the total NCAPG2 protein level in each genotype. Total NCAPG2 protein levels were equivalent among *domesticus*, *spretus* and hybrid oocytes. For gel source data, see Supplementary Fig. 1. **d**, *domesticus*, *musculus*, *spretus* and *spicilegus* oocytes were fixed at

prophase I and stained for NCAPG2. NCAPG2 intensities in the nucleus were quantified; each dot in the graph represents a single oocyte (n = 18, 24, 21 and 33 oocytes for *domesticus*, *musculus*, *spretus* and *spicilegus*, respectively); unpaired t-test (two-sided) was used for statistical analysis; ***P < 0.0001. Images are optical slices to show the nucleus. **e**, Chromosome spreads were performed at metaphase I using *domesticus*, *spicilegus* and *domesticus* × *spicilegus* hybrid oocytes expressing MajSat and counterstained with DAPI. Centromeric MajSat intensities were quantified in *domesticus* and *spicilegus* oocytes (n = 488 and 354 centromeres for *domesticus* and *spicilegus*, respectively); unpaired t-test (two-sided) was used for statistical analysis; ****P < 0.0001. Centromere MajSat signal ratios in *domesticus* × *spicilegus* hybrid oocytes were calculated as the *domesticus* centromere divided by the *spicilegus* centromere signal for each bivalent (n = 183 chromosomes); each dot in the graph represents a single bivalent chromosome. The quantification shows that *spicilegus* centromeres have less major satellites compared to *domesticus* ones, consistent with a previous study using dot-plot hybridization⁵⁸. Images are maximum intensity z projections to show all chromosomes or optical slices to show individual chromosomes; red line, mean; scale bars: 5 μm.

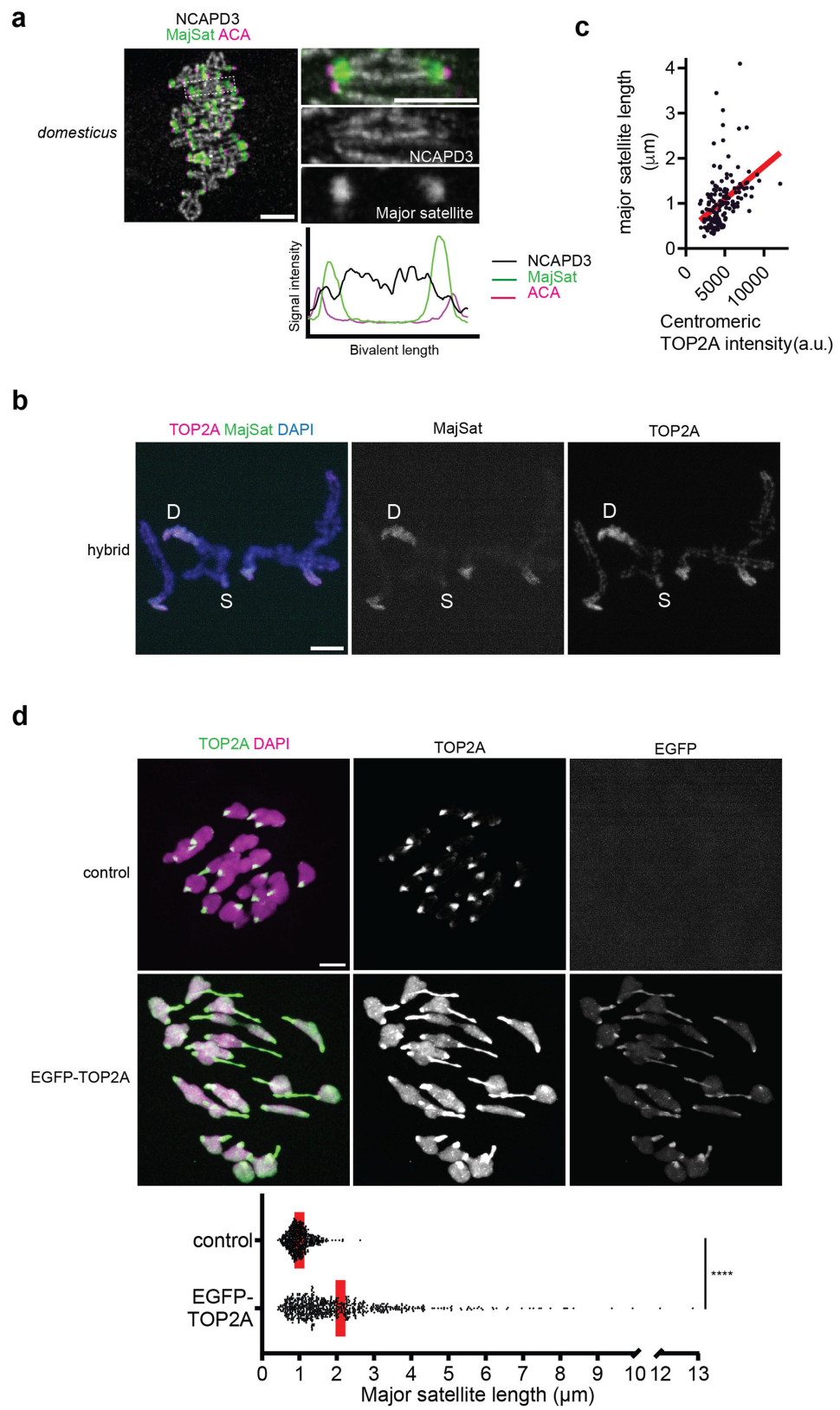
Article



Extended Data Fig. 7 | See next page for caption.

Extended Data Fig. 7 | NCAPG2 nuclear enrichment is critical for timely chromosome condensation in mouse oocytes. **a**, Hybrid oocytes expressing *spretus* NCAPG2-eGFP were fixed at metaphase I and stained for NCAPD3 and eGFP. NCAPD3 intensities on chromosomes were quantified (n = 61 and 48 oocytes for control and *spretus* NCAPG2-eGFP, respectively); unpaired t-test (two-sided) was used for statistical analysis; *P = 0.0423. **b**, Hybrid oocytes expressing *domesticus* NCAPG2-eGFP, *spretus* NCAPG2-eGFP or *spretus* NCAPG2-NES-eGFP were fixed at prophase I and stained for eGFP. Nuclear/cytoplasmic ratios of eGFP intensities were quantified; each dot in the graph represents a single oocyte (n = 37, 31, 40 and 29 oocytes for control, *domesticus* NCAPG2-eGFP, *spretus* NCAPG2-eGFP and *spretus* NCAPG2-NES-eGFP, respectively); unpaired t-test (two-sided) was used for statistical analysis; ***P < 0.0001. **c**, Hybrid oocytes expressing *spretus* NCAPG2-eGFP or *spretus* NCAPG2-NES-eGFP were fixed at prophase I and stained for NCAPG2 and eGFP. NCAPG2 intensities in the nucleus were quantified; each dot in the graph represents a single oocyte (n = 16, 25 and 30 oocytes for control, *spretus* NCAPG2-eGFP and *spretus* NCAPG2-NES-eGFP, respectively); unpaired t-test

(two-sided) was used for statistical analysis; *P = 0.0165, ***P < 0.0001. Specifically, the *spretus* NCAPG2-eGFP overexpression increased the total NCAPG2 levels in the nucleus. **d**, Hybrid oocytes expressing *spretus* NCAPG2-eGFP or *spretus* NCAPG2-NES-eGFP were fixed either at prometaphase I or metaphase I and stained for eGFP and TOP2A. White arrowheads indicate stretched centromeres. eGFP intensities on chromosomes (prometaphase I: n = 37, 37 and 25 oocytes for control, *spretus* NCAPG2-eGFP and *spretus* NCAPG2-NES-eGFP, respectively; metaphase I: n = 61, 48 and 43 oocytes for control, *spretus* NCAPG2-eGFP and *spretus* NCAPG2-NES-eGFP, respectively; each dot represents a single oocyte) and the major satellite length in prometaphase I were quantified (n = 488, 549 and 368 chromosomes for control, *spretus* NCAPG2-eGFP and *spretus* NCAPG2-NES-eGFP, respectively; each dot represents a single centromere); unpaired t-test (two-sided) was used for statistical analysis; ***P < 0.0001. Images are maximum intensity z projections to show all chromosomes or optical slices to show individual chromosomes; red line, mean; scale bars: 5 μm.

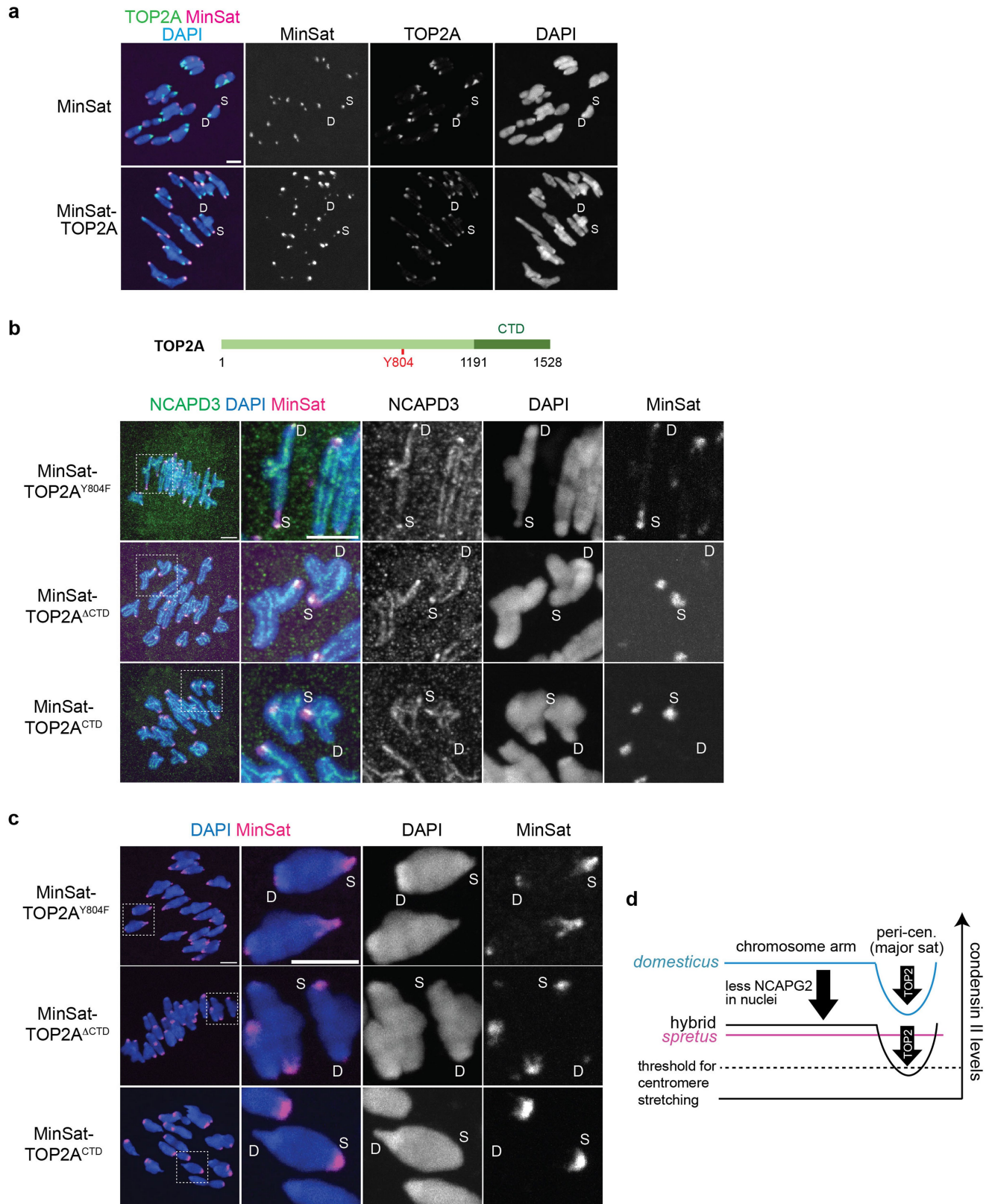


Extended Data Fig. 8 | See next page for caption.

Extended Data Fig. 8 | High TOP2A and low condensin II abundance at major satellites. **a**, *domesticus* oocytes expressing MajSat were fixed at metaphase I and stained for NCAPD3 (antibody from the Hirano lab). The graph is line scans of MajSat (green), centromere (magenta), and NCAPD3 (black) intensities across the chromosome length. Major satellites had reduced levels of condensin II compared to the rest of the chromosome in both *domesticus* and hybrid (Fig. 4a) oocytes, indicating that condensin II has an intrinsic property of loading less on major satellites. This experiment was repeated independently two times with similar results. **b**, Chromosome spreads were performed at metaphase I using hybrid oocytes expressing MajSat and stained for TOP2A. “D” and “S” indicate *domesticus* and *spretus* centromeres, respectively. *domesticus* centromeres with major satellites highly enrich

TOP2A compared to *spretus* centromeres. This experiment was repeated independently two times with similar results. **c**, Images taken for Fig. 4b were re-analysed to plot the centromeric TOP2A intensities relative to the length of major satellites on each chromosome ($n = 159$ chromosomes); red line, a simple linear regression between the centromeric TOP2A intensities and the length of major satellites ($R^2 = 0.1784, P < 0.001$). **d**, Hybrid oocytes expressing eGFP-TOP2A were fixed at prometaphase I and stained for TOP2A and eGFP. The major satellite length was quantified ($n = 543$ and 653 centromeres for control and eGFP-TOP2A, respectively); unpaired t-test (two-sided) was used for statistical analysis, $****P < 0.0001$. Overexpressing TOP2A enhanced the centromere stretching phenotype rather than rescuing it. Images are maximum intensity z projections to show all chromosomes; red line, mean; scale bars: 5 μm .

Article



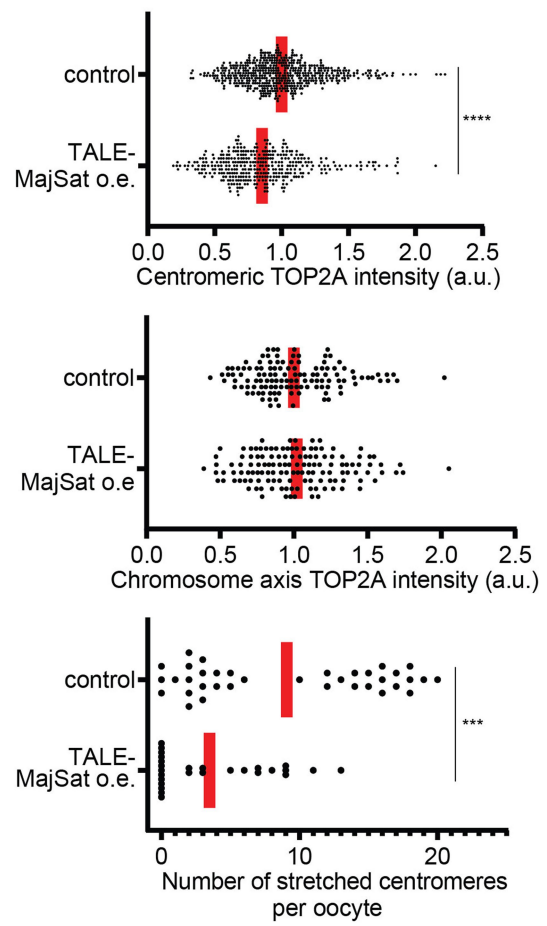
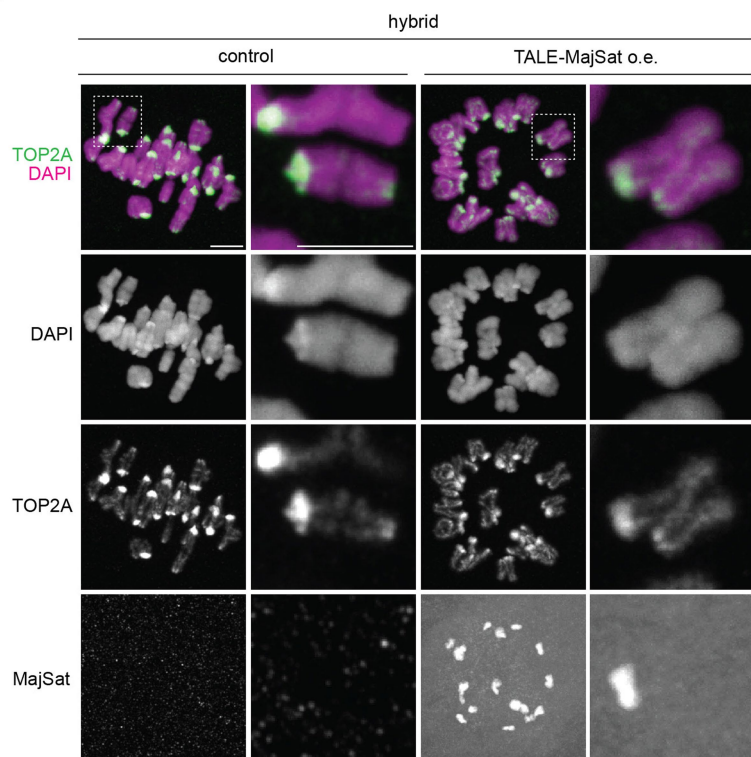
Extended Data Fig. 9 | See next page for caption.

Extended Data Fig. 9 | TOP2A's catalytic activity and its guiding function to localize to the chromosome axis are critical to reduce condensin II abundance at centromeres. **a**, Hybrid oocytes expressing MinSat or MinSat-TOP2A were fixed at prometaphase I and stained for TOP2A. TOP2A levels recruited to *spretus* centromeres by this targeting strategy was equivalent to that on major satellites. This experiment was repeated independently two times with similar results. **b,c**, Hybrid oocytes expressing MinSat-TOP2A^{Y804F}, MinSat-TOP2A^{ACTD} or MinSat-TOP2A^{CTD} were fixed either at metaphase I and stained for NCAPD3 (**b**) or fixed at prometaphase I and counterstained with DAPI (**c**). These experiments were repeated independently two to four times with similar results. MinSat-TOP2A^{Y804F}, MinSat-TOP2A^{ACTD} and MinSat-TOP2A^{CTD} were less efficient in reducing condensin II abundance and

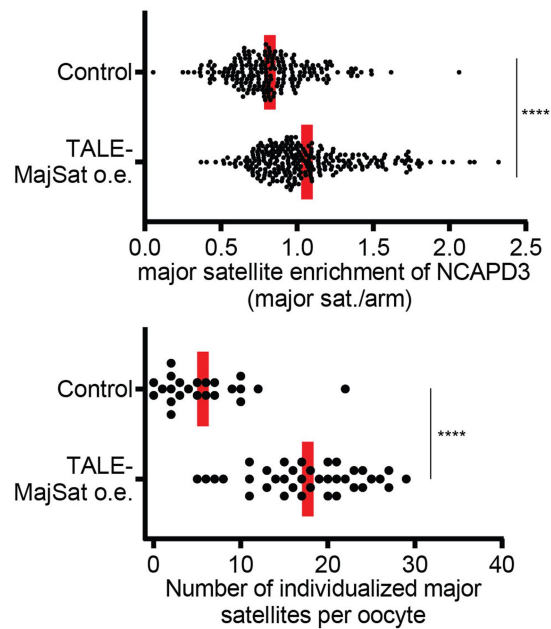
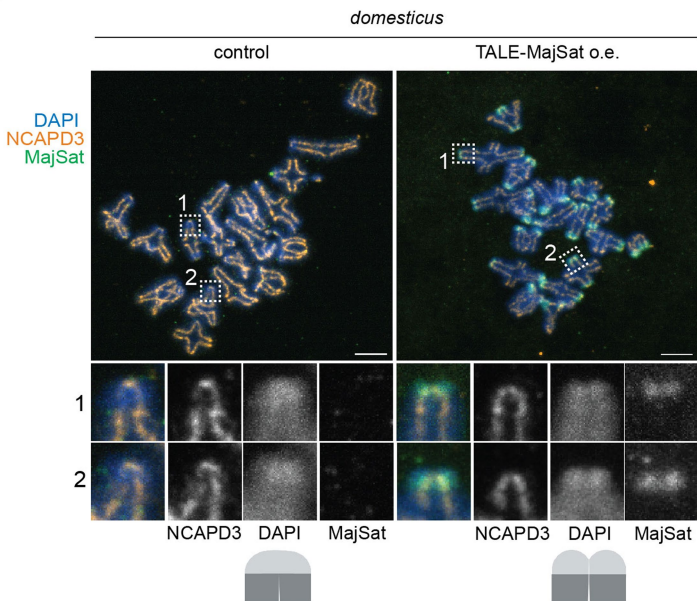
inducing centromere stretching compared to MinSat-TOP2A (wild-type), indicating that both TOP2A's catalytic activity and its guiding function to localize to the chromosome axis are important to reduce condensin II abundance at centromeres⁶². “D” and “S” indicate *domesticus* and *spretus* centromeres, respectively. Images are maximum intensity z projections to show all chromosomes (left) or optical slices magnified to show individual chromosomes (right). Scale bar: 5 μm. **d**, Schematic showing two pathways that regulate condensin II levels. Nuclear NCAPG2 levels dictate the condensin II abundance on the overall chromosome, while major satellites locally reduce condensin II abundance via TOP2A. *spretus* pericentromeres have very little major satellites, maintaining their centromeres compact despite they have lower basal condensin II levels on the chromosome.

Article

a



b



Extended Data Fig. 10 | See next page for caption.

Extended Data Fig. 10 | Major satellite-specific TOP2A reduction increases condensin II at major satellites and rescues centromere stretching. **a**, Hybrid oocytes over-expressing MajSat were fixed at prometaphase I and stained for TOP2A. Centromeric TOP2A levels (top graph; n = 528 and 361 centromeres for control and MajSat o.e., respectively; each dot represents a single centromere), chromosome axis TOP2A levels (middle graph; n = 124 and 133 chromosomes for control and MajSat o.e., respectively; each dot represents a single chromosome), and the number of stretched centromere per oocyte (bottom graph; n = 36 and 27 oocytes for control and MajSat o.e., respectively; each dot represents a single oocyte) were quantified; unpaired t-test (two-sided) was used for statistical analysis; ***P = 0.0004, ****P < 0.0001. **b**, *domesticus*

oocytes over-expressing MajSat were fixed at metaphase I and stained for NCAPD3. Graphs show major satellite enrichment of NCAPD3, calculated as the signal at major satellite divided by the chromosome arm signal for each half-bivalent (top graph; n = 210 and 262 for control and MajSat o.e., respectively) or individualization of sister chromatids at major satellites based on the DAPI staining (bottom graph; n = 23 and 37 for control and MajSat o.e., respectively); unpaired t-test (two-sided) was used for statistical analysis; ***P < 0.0001. Images are maximum intensity z projection to show all chromosomes or optical slices magnified to show individual chromosomes; red line, mean, scale bar: 5 μ m.

Reporting Summary

Nature Portfolio wishes to improve the reproducibility of the work that we publish. This form provides structure for consistency and transparency in reporting. For further information on Nature Portfolio policies, see our [Editorial Policies](#) and the [Editorial Policy Checklist](#).

Statistics

For all statistical analyses, confirm that the following items are present in the figure legend, table legend, main text, or Methods section.

n/a Confirmed

- The exact sample size (n) for each experimental group/condition, given as a discrete number and unit of measurement
- A statement on whether measurements were taken from distinct samples or whether the same sample was measured repeatedly
- The statistical test(s) used AND whether they are one- or two-sided
Only common tests should be described solely by name; describe more complex techniques in the Methods section.
- A description of all covariates tested
- A description of any assumptions or corrections, such as tests of normality and adjustment for multiple comparisons
- A full description of the statistical parameters including central tendency (e.g. means) or other basic estimates (e.g. regression coefficient) AND variation (e.g. standard deviation) or associated estimates of uncertainty (e.g. confidence intervals)
- For null hypothesis testing, the test statistic (e.g. F , t , r) with confidence intervals, effect sizes, degrees of freedom and P value noted
Give P values as exact values whenever suitable.
- For Bayesian analysis, information on the choice of priors and Markov chain Monte Carlo settings
- For hierarchical and complex designs, identification of the appropriate level for tests and full reporting of outcomes
- Estimates of effect sizes (e.g. Cohen's d , Pearson's r), indicating how they were calculated

Our web collection on [statistics for biologists](#) contains articles on many of the points above.

Software and code

Policy information about [availability of computer code](#)

Data collection All images were collected using NIS-Elements imaging software (Nikon)

Data analysis Fiji/ImageJ (NIH) (version: 2.14.0/1.54f) was used to analyze all the images, and Microsoft Excel (version: 16.76) and GraphPad Prism 10 (version: 10.0.0) were used for statistical analyses.

For manuscripts utilizing custom algorithms or software that are central to the research but not yet described in published literature, software must be made available to editors and reviewers. We strongly encourage code deposition in a community repository (e.g. GitHub). See the Nature Portfolio [guidelines for submitting code & software](#) for further information.

Data

Policy information about [availability of data](#)

All manuscripts must include a [data availability statement](#). This statement should provide the following information, where applicable:

- Accession codes, unique identifiers, or web links for publicly available datasets
- A description of any restrictions on data availability
- For clinical datasets or third party data, please ensure that the statement adheres to our [policy](#)

The datasets generated and/or analyzed during the current study are available in figshare at doi: 10.25444/nhlbi.23671194

Human research participants

Policy information about [studies involving human research participants](#) and [Sex and Gender in Research](#).

Reporting on sex and gender

N/A

Population characteristics

N/A

Recruitment

N/A

Ethics oversight

N/A

Note that full information on the approval of the study protocol must also be provided in the manuscript.

Field-specific reporting

Please select the one below that is the best fit for your research. If you are not sure, read the appropriate sections before making your selection.

Life sciences Behavioural & social sciences Ecological, evolutionary & environmental sciences

For a reference copy of the document with all sections, see nature.com/documents/nr-reporting-summary-flat.pdf

Life sciences study design

All studies must disclose on these points even when the disclosure is negative.

Sample size

No statistical methods were used to predetermine sample size. The sample size was chosen based on current practices in the field. Between 10 - 100 oocyte cells were analyzed per biological replicate, depending on the type of experiment (live-cell imaging, fixed-cell imaging, westernblot). The sample size was determined to have sufficient statistical power.

Data exclusions

No data were excluded from the analysis except for Fig. 4a and 4d where we focused our analyses on hybrid oocytes with detectable NCAPD3 levels on the chromosome to analyze their localization pattern within the chromosome.

Replication

All attempts of replication were successful. Data points were pooled from two to five independent experiments (biological replicates). The exact number of experiments for each experimental group is listed in Supplementary Table 1.

Randomization

Randomization is built into our experiments because each animal was chosen from a different litter and mating pair and no data was excluded and all cells were imaged at random.

Blinding

Investigators were not blinded for data collection (imaging) and quantifications (data analysis) as the phenotype automatically reports on the genotype consistently and is very penetrant.

Reporting for specific materials, systems and methods

We require information from authors about some types of materials, experimental systems and methods used in many studies. Here, indicate whether each material, system or method listed is relevant to your study. If you are not sure if a list item applies to your research, read the appropriate section before selecting a response.

Materials & experimental systems

n/a	Involved in the study
<input type="checkbox"/>	<input checked="" type="checkbox"/> Antibodies
<input checked="" type="checkbox"/>	<input type="checkbox"/> Eukaryotic cell lines
<input checked="" type="checkbox"/>	<input type="checkbox"/> Palaeontology and archaeology
<input type="checkbox"/>	<input checked="" type="checkbox"/> Animals and other organisms
<input checked="" type="checkbox"/>	<input type="checkbox"/> Clinical data
<input checked="" type="checkbox"/>	<input type="checkbox"/> Dual use research of concern

Methods

n/a	Involved in the study
<input checked="" type="checkbox"/>	<input type="checkbox"/> ChIP-seq
<input checked="" type="checkbox"/>	<input type="checkbox"/> Flow cytometry
<input checked="" type="checkbox"/>	<input type="checkbox"/> MRI-based neuroimaging

Antibodies

Antibodies used

The following primary antibodies were used: rabbit anti-mouse NCAPD3 antibody (Fig. 2b, 3a, 4a, 4d, Extended Data Figs. 2b, 8a, 9b, 1:500, gift from Dr. T. Hirano), rabbit anti-mouse NCAPG antibody (1:500, gift from Dr. T. Hirano) rabbit anti-human NCAPD3 (Fig. 5b)

and Extended Data Fig. 2a, 7a, 1:100, Bethyl, cat# A300-604A), rabbit anti-human NCAPG2 (Fig. 3a, 1:100; Bioss, cat# BS-7721R), rabbit anti-human NCAPG2 (Extended Data Fig. 6b, 6d, 1:100, Bethyl, cat# A300-605A), rabbit anti-human NCAPH2 (1:100, Bethyl, cat# A302-275A), goat anti-human CAPE (SMC2) (1:100, Abcepta, cat# AF2276a), rabbit anti-mouse SMC4 (1:100, Novus, cat# NBP1-86635), CREST human autoantibody against centromere (1:100, Immunovision, cat# HCT-0100), rabbit anti-Topoisomerase II (1:100, Abcam, cat# ab109524), goat anti-GFP antibody conjugated with Dylight488 (1:100, Rockland, cat# 600-141-215). Secondary antibodies were Alexa Fluor 488-conjugated donkey anti-rabbit (1:500, Invitrogen, cat# A21206) or donkey anti-goat (1:500, Invitrogen, cat# A11057), Alexa Fluor 568-conjugated goat anti-rabbit (1:500, Invitrogen, cat# A10042), or Alexa Fluor 647-conjugated goat anti-human (1:500, Invitrogen, cat# A21445). Normal rabbit IgG (Sigma-Aldrich, cat# 12-370) and rabbit anti-human NCAPH2 antibody (Invitrogen, cat# pa5-66964) were used for the TrimAway method at 0.2 mg/ml.

Validation

Two antibodies recognizing different NCAPD3 epitopes were used in this study, and both showed similar staining patterns: rabbit anti-mouse NCAPD3 antibody (Fig. 2b, 3a, 4a, 4d, Extended Data Figs. 2b, 8a, 9b) is a gift from Dr. T. Hirano (Lee J et al. MBoC, 2011), and rabbit anti-human NCAPD3 antibody (Fig. 5b and Extended Data Fig. 2a, 7a, Bethyl, cat# A300-604A) was previously used in (Boteva L et al. Cell Rep, 2020).

The NCAPG antibody is a gift from Dr. T. Hirano (Lee J et al. MBoC, 2011) and validated for the use for immunofluorescence analysis.

Two antibodies recognizing different NCAPG2 epitopes were used in this study, and both showed similar staining patterns in the nucleus: rabbit anti-human NCAPG2 antibody (Extended Data Fig. 6b, 6d, 1:100, Bethyl, cat# A300-605A) was previously used in (Kong M et al. Mol Cell, 2020), and rabbit anti-human NCAPG2 antibody (Fig. 3a, 1:100; Bioss, cat# BS-7721R) is recommended by the manufacturer for the use in immunostaining and western blot and has been validated for these applications in this study.

The rabbit anti-human NCAPH2 Bethyl, cat# A302-275A was previously validated in multiple studies, including (Elbatsh AMO et al. Mol Cell, 2019)

The goat anti-human CAPE (SMC2) (Abcepta, cat# AF2276a) was validated for the use in immunostaining in this study.

The rabbit anti-mouse SMC4 (1:100, Novus, cat# NBP1-86635) have been previously validated in mouse oocytes (Hwang G et al. Development, 2017).

The CREST human autoantibody against centromere (1:100, Immunovision, cat# HCT-0100) is commonly used to stain centromeres in somatic cells and germline cells in mammals.

The rabbit anti-Topoisomerase II (1:100, Abcam, cat# ab109524) have been previously validated in mouse oocytes (Mengoli V et al. EMBO J, 2021).

Normal rabbit IgG (Sigma-Aldrich, cat# 12-370); see manufacturer's website for references and validation (<https://www.sigmaaldrich.com/US/en/product/mm/12370>)

Rabbit anti-human NCAPH2 antibody (Invitrogen, cat# pa5-66964); see manufacturer's website for references and validation (<https://www.thermofisher.com/antibody/product/NCAPH2-Antibody-Polyclonal/PAA5-66964>)

Animals and other research organisms

Policy information about [studies involving animals](#); [ARRIVE guidelines](#) recommended for reporting animal research, and [Sex and Gender in Research](#)

Laboratory animals

Mouse strains were purchased from Envigo (NSA, stock# 033 corresponds to CF1, *Mus musculus domesticus*), from Jackson Laboratory (C57BL/6J, stock# 000664, *Mus musculus domesticus*, PWD/PhJ, stock# 004660, *Mus musculus musculus*), and from RIKEN BioResource Research Center (SPR2, stock# RBRC00208, *Mus spretnus*, ZBN/Ms, stock# RBRC00661, *Mus spicilegus*). All mice used in this study were between 6 to 12 week old.

Wild animals

No wild animal were used in this study.

Reporting on sex

We only used female mice, because we study female meiosis.

Field-collected samples

This study does not involve sample collections from the field.

Ethics oversight

All animal experiments were approved by the Animal Care and Use Committee (National Institutes of Health Animal Study Proposal#: H-0327) and were consistent with the National Institutes of Health guidelines.

Note that full information on the approval of the study protocol must also be provided in the manuscript.